

Experimental study on hard radiation from long laboratory spark discharges in air

Citation for published version (APA):

Nguyen, C. V. (2012). *Experimental study on hard radiation from long laboratory spark discharges in air*. [Phd Thesis 1 (Research TU/e / Graduation TU/e), Electrical Engineering]. Technische Universiteit Eindhoven. <https://doi.org/10.6100/IR731153>

DOI:

[10.6100/IR731153](https://doi.org/10.6100/IR731153)

Document status and date:

Published: 01/01/2012

Document Version:

Publisher's PDF, also known as Version of Record (includes final page, issue and volume numbers)

Please check the document version of this publication:

- A submitted manuscript is the version of the article upon submission and before peer-review. There can be important differences between the submitted version and the official published version of record. People interested in the research are advised to contact the author for the final version of the publication, or visit the DOI to the publisher's website.
- The final author version and the galley proof are versions of the publication after peer review.
- The final published version features the final layout of the paper including the volume, issue and page numbers.

[Link to publication](#)

General rights

Copyright and moral rights for the publications made accessible in the public portal are retained by the authors and/or other copyright owners and it is a condition of accessing publications that users recognise and abide by the legal requirements associated with these rights.

- Users may download and print one copy of any publication from the public portal for the purpose of private study or research.
- You may not further distribute the material or use it for any profit-making activity or commercial gain
- You may freely distribute the URL identifying the publication in the public portal.

If the publication is distributed under the terms of Article 25fa of the Dutch Copyright Act, indicated by the "Taverne" license above, please follow below link for the End User Agreement:

www.tue.nl/taverne

Take down policy

If you believe that this document breaches copyright please contact us at:

openaccess@tue.nl

providing details and we will investigate your claim.

Experimental Study on Hard Radiation from Long Laboratory Spark Discharges in Air

PROEFSCHRIFT

ter verkrijging van de graad van doctor aan de
Technische Universiteit Eindhoven, op gezag van de
rector magnificus, prof.dr.ir. C.J. van Duijn, voor een
commissie aangewezen door het College voor
Promoties in het openbaar te verdedigen
op woensdag 18 april 2012 om 16.00 uur

door

Cung Vuong Nguyen

geboren te Phu Khanh, Vietnam

Dit proefschrift is goedgekeurd door de promotoren:

prof.dr.ir. J.H. Blom

en

prof.ir. W.L. Kling

Copromotor:

dr. A.P.J. van Deursen

A catalogue record is available from the Eindhoven University of Technology
Library ISBN: 978-90-386-3123-3

...To my parents and my family

Samenstelling promotiecommissie:

Promotoren:

prof.dr.ir. J.H. Blom, Technische Universiteit Eindhoven

prof.ir. W.L. Kling, Technische Universiteit Eindhoven

Copromotor:

dr. A.P.J. van Deursen, Technische Universiteit Eindhoven

Kerncommissie:

prof.dr. U.M. Ebert, Technische Universiteit Eindhoven and CWI Amsterdam

prof.dr. N. Østgaard, University of Bergen

dr. T. Neubert, Technical University of Denmark (DTU Space)

Andere leden:

prof.dr.ir. G.M.V. Kroesen, Technische Universiteit Eindhoven

prof.dr.ir. A.C.P.M. Backx (voorzitter), Technische Universiteit Eindhoven

	Summary	v
	Samenvatting	ix
1	Introduction	1
1.1	Electrical discharges	1
1.2	History of the problem	2
1.2.1	Streamers	2
1.2.2	Long laboratory Spark discharges	3
1.2.3	X/ γ -rays from atmospheric origin	4
1.2.4	Runaway breakdown	6
1.3	Motivation and scope of this study	6
1.4	Research goals	7
1.5	Scientific approach	8
1.6	Structure of the thesis	9
2	X-ray detectors	11
2.1	Introduction	11
2.2	Scintillation detectors	12
2.2.1	Introduction to scintillation detectors	12
2.2.2	NaI(Tl) scintillation detector	16
2.2.3	BaF ₂ scintillation detector	17
2.2.4	LaBr ₃ (Ce ⁺) scintillation detector	18
2.2.4.1	Linearity of the LaBr ₃ (Ce ⁺) scintillation detector	21
2.3	Cadmium Zinc Telluride semiconductor detector	24
2.3.1	Introduction to semiconductor detector	24

2.3.2	Preliminary X-ray measurements with a pixelated CZT detector	26
2.4	Discussion and conclusions	28
3	X-ray from wire-plate corona reactor	31
3.1	Introduction	31
3.2	Experimental set-up and procedure	32
3.3	The streamer phase	34
3.4	X-ray detection	35
3.5	Discussion	39
3.6	Conclusion	39
4	Multiple X-ray bursts from long discharges in air	41
4.1	Introduction	41
4.2	Experimental set-up and procedure	42
4.2.1	γ -detectors	44
4.3	Experimental data	46
4.3.1	Comparison of γ -detectors	46
4.3.2	Positive high voltage surges	47
4.3.3	Negative high voltage surges	49
4.3.4	Distance variation	50
4.3.5	Absorber	51
4.4	Discussion and conclusion	52
5	Observation of X-ray bursts in meter-long discharges associated with negative streamer initiation	55
5.1	Introduction	55
5.2	Experimental set-up and procedure	56
5.3	Experimental data	59
5.3.1	Results for positive high voltage surges	60
5.3.2	Results for negative high voltage surges	64
5.4	Discussion and conclusion	67
6	General conclusions and recommendations	71
6.1	X-ray detectors	71
6.2	X-rays from streamer-corona plasma	72
6.3	Metre-long spark discharges in air	72
6.4	Recommendations for future work	73
	Bibliography	75
	List of Publications	87

Acknowledgements	89
Curriculum Vitae	91

SUMMARY

The detection of hard radiation emanating from an electrical discharge in air is still a mysterious phenomenon. This thesis focuses on collecting experimental data around spark condition that could lead to the production of energetic photon bursts. Long spark discharges with positive and negative polarity in air are studied. We accurately measure the electrical currents on both electrodes during the formation of the discharge. The X-rays are detected with scintillation detectors, time synchronized with the electrical parameters. Bursts up to several 100 keV photons are observed. The advantage of ‘laboratory lightning’ is the controlled environment that allows to study the distribution of the X-rays in space and time.

The experiments are performed in the high voltage laboratory at Eindhoven University of Technology. A 2 MV twelve stage Marx generator, with a standardized lightning impulse with 1.2/50 μ s rise/decay time to half-maximum when unloaded, delivers the high voltage air breakdown. A 9 m tall 1:2000 capacitive high voltage divider (part of the waveshaping circuit) is used to monitor the voltage waveform produced by the Marx generator. The generator is connected to a spark gap with two conical electrodes at distances varying between 0.76 and 1.46 m. The current at the grounded electrode is measured by a Pearson current probe. An identical probe around the high voltage electrode was connected through a fiber optical data transmission system for electrical isolation. Electromagnetic disturbance from the discharge itself was reduced to a negligible level in the measurements by proper design of the cables and protection equipment.

Fast X-ray detectors with good energy resolution are imperative for reliable X-ray registrations. We use conventional NaI(Tl), nanosecond fast BaF₂ and

two newly developed $\text{LaBr}_3(\text{Ce}^+)$ scintillation detectors, all with suitable photo-multiplier integrated. Later the DTU National Space Institute assisted in the experiments with a test Cadmium Zinc Telluride (CZT) semiconductor detector intended for the Atmosphere-Space Interactions Monitor (ASIM) project.

In early measurements partial discharges at unexpected positions occurred that could also produce X-rays. This effect could be controlled by covering sharp protrusions with conducting foil.

The currents measured through both electrodes differ substantially during the first few microseconds. This is caused by the Ramo-Shockley effect. In the development phase of the discharge a charge cloud developed around the high voltage electrode and most of the associated electric field lines end in the environment of the grounded electrode, but not on the electrode. Through this current difference between both electrodes it was possible to tell where burst of X-rays are formed. For both polarities of the high voltage, the bursts of X-rays are associated with the negative streamer formation at the cathode. For positive polarity surges X-ray bursts detected coincide with the onset of the upward negative streamer prior to the bridging of the electrode distance. In the case of negative polarity surges X-ray bursts coincide with the negative streamers immediately at the onset of the spark formation. No X-rays have been detected during the large current of the gap breakdown. At gap breakdown both currents become equal.

In a parallel investigation we confirmed that the $\text{LaBr}_3(\text{Ce}^+)$ scintillation detector suited best for our experimental study because of the short decay time compared with $\text{NaI}(\text{Tl})$ and the better energy resolution compared with BaF_2 . Still, we found that pile-up of multiple photons and/or electrons can occur in the $\text{LaBr}_3(\text{Ce}^+)$ detectors in the 23 ns of the $1/e$ decay. The $\text{LaBr}_3(\text{Ce}^+)$ detector has been calibrated and tested for its linearity at photon energies between 59.5 and 2505 keV, employing photomultiplier bias voltages from 568 up to 1000 V.

Preliminary X-ray measurements with a small CZT semiconductor detector gave no conclusive results due to the poor detection events (6 out of 100) obtained. Additional experiments with a larger detector for higher detection rates are recommended for a better understanding of the particle distributions involved.

An additional experiment was carried out to confirm the emission of X-ray during the streamer phase of an electrical discharge in air. Streamer filaments were produced in a small streamer-corona reactor with nanosecond high voltage pulses up to 65 kV with an optional 20 kV_{dc} offset. The short high voltage pulse period prevents the streamers to develop into an air breakdown. The $\text{LaBr}_3(\text{Ce}^+)$ scintillation detector recorded X-rays from the streamer filaments with very

consistent timing of occurrences. This proves that processes near the streamers heads are able to produce X-rays.

Various results were presented at a number of international conferences and workshops. Chapter 3 and Chapter 4 have been published in Journal of Physics D: Applied Physics.

SAMENVATTING

De detectie van hoog energetische straling afkomstig van een elektrische ontlading in lucht is nog steeds een raadselachtig fenomeen. Dit proefschrift is gericht op het experimenteel verzamelen van data rondom boogontladingen waarbij emissies van hoog energetische fotonen kunnen optreden. Lange boogontladingen met positieve en negatieve polariteit in lucht zijn bestudeerd. De elektrische stromen door beide elektroden tijdens de boog vorming worden nauwkeurig gemeten. Tegelijkertijd wordt de gegenereerde röntgenfotonen met scintillatiedetectoren gemeten. Foton-energieën tot enkele 100 keV zijn waargenomen. Het voordeel van 'laboratorium bliksem' is de gecontroleerde omgeving die het mogelijk maakt om plaats en tijd opgeloste verdeling van röntgenfotonen te bestuderen.

De experimenten zijn uitgevoerd in het hoogspanningslaboratorium van de faculteit elektrotechniek aan de Technische Universiteit Eindhoven. Een 2 megavolt twaalf traps Marx generator, met een gestandaardiseerde bliksem impuls signaalvorm met $1.2/50 \mu\text{s}$ stijg-/vervaltijd bij half-maximum wanneer onbelast, levert de hoge spanning voor doorslag in lucht. Een 9 m hoge 1:2000 capacitieve hoogspanningsdeler (onderdeel van het waveshaping circuit) wordt gebruikt om de spanningsgolfvorm die door de Marx generator wordt geproduceerd te monitoren. De generator is aangesloten op een conische elektroden configuratie met tussenafstanden variërend van 0.76 tot en met 1.46 m. De stroom door de gearde elektrode is met een Pearson stroom sensor gemeten. Een identieke stroom sensor aan de zijde van de hoogspanningselektrode is aangesloten via een optisch datatransmissie systeem in verband met hoogspanningsisolatie. Door specifieke maatregelen te nemen bij het aansluiten van de kabels en afscherming van de apparatuur is de elektromagnetische storing van de ontlading zelf gereduceerd tot een verwaarloosbaar niveau tijdens de metingen.

Snelle röntgendetectoren met een goede energie resolutie zijn noodzakelijk voor betrouwbare registratie van röntgenfotonen. We gebruikten de conventionele NaI(Tl), de nanoseconde snelle BaF₂ en nieuw ontwikkelde LaBr₃(Ce⁺) scintillatiedetectoren, elk met geschikte fotomultipliers geïntegreerd. Later droeg het DTU National Space Institute aan de experimenten bij met een speciale Cadmium Zink Telluride (CZT) halfgeleider detector bestemd voor het Atmosphere-Space Interactions Monitor (ASIM) project.

In de eerste metingen traden partiële ontladingen op op onverwachte locaties waardoor er ook op die plaatsen röntgenfotonen kan worden geproduceerd. Dit effect kon worden opgelost door op desbetreffende plekken de uitsteeksels met geleidende folie af te vlakken.

De gemeten stromen door beide elektroden verschillen sterk tijdens de eerste paar microseconden. Dit komt door het Ramo-Shockley effect. In de fase van de boogvorming accumuleert zich een volume van ladingsdichtheid rond de hoogspanningselektrode waardoor het grootste gedeelte van de bijbehorende elektrische veldlijnen eindigt op de omgeving van de geaarde elektrode, maar niet op de aardelektrode zelf. Dankzij dit verschil in stroomwaarden tussen de beide elektroden is het mogelijk gebleken om te bepalen waar de emissie van röntgenfotonen plaats vindt. Voor positieve en negatieve hoogspanning, worden de röntgenfoton emissies geassocieerd met de negatieve streamer formatie op de kathode. Voor positieve polariteit boogontladingen vallen de gedetecteerde röntgenfoton emissies samen met het begin van de opwaartse negatieve streamer voorafgaand aan de overbrugging van de elektrode afstand. In het geval van negatieve polariteit boogontladingen valt de röntgenfoton emissies samen met de negatieve streamers bij aanvang van de boogvorming. Geen röntgenfotonen werden gedetecteerd tijdens de fikse korstsluitstroom. Bij volledige doorslag is de stroom amplitude is gelijk.

In een parallel onderzoek hebben we bevestigd dat de LaBr₃(Ce⁺) scintillatiedetector het meest geschikt is voor gebruikt bij onze experimentele studie vanwege de korte respons tijdsduur in vergelijking met NaI(Tl) en de betere energie resolutie vergeleken met BaF₂. Desondanks zagen we met de LaBr₃(Ce⁺) detectoren dat opeenstapeling van meerdere fotonen en/of elektronen pulsen kunnen optreden binnen de 1/e vervaltijd van 26 ns. De LaBr₃(Ce⁺) detector is gekalibreerd en getest op zijn lineariteit met foton energieën tussen de 59.5 en 2505 keV, met fotomultiplier voedingsspanningen variërend van 568 tot 1000 V.

Voorlopige metingen met een kleine CZT halfgeleider detector leverde geen conclusieve resultaten op vanwege de lage detectie van röntgenfotonen (6 uit 100). Uitgebreidere experimenten met een grotere detector voor een hogere detectiekans is aan te bevelen om een beter inzicht te verkrijgen in de distributie van de deeltjes.

Een aanvullend experiment is uitgevoerd om te bevestigen dat de productie van röntgenfotonen kan optreden tijdens de streamer fase van een elektrische ontlading in lucht. Streamer filamenten zijn gegenereerd in een kleine streamer-corona reactor door het toepassen van nanoseconden hoogspanningspulsen tot 65 kV met een optionele superpositie van 20 kV_{dc} offset. De korte hoogspanningspuls duurt zo kort dat de streamers zich verder ontwikkelen tot een volledige doorslag in lucht. De LaBr₃(Ce⁺) scintillatiedetector registreerde röntgenfotonen afkomstig van de streamer filamenten met een zeer consistent tijdstip van optreden. Dit toont aan dat processen in de omgeving van de streamerkop in staat zijn om röntgenfotonen te produceren.

Verscheidene resultaten zijn gepresenteerd op een aantal internationale conferenties en workshops. Hoofdstuk 3 en hoofdstuk 4 zijn gepubliceerd in Journal of Physics D: Applied Physics.

CHAPTER 1

INTRODUCTION

The main topic of this thesis is the experimental study of the emission of bursts of hard radiation (or X-rays) from long spark discharges in air generated in a high voltage laboratory. Under normal conditions a spark discharge begins with the formation of streamer filaments from which multiple channels develop into the air gap. These streamers ultimately bridge the electrode gap distance and initiate a total gap breakdown. The investigation is focussed on the early stage of spark development, where streamer channels are formed. The emission of X-ray bursts only occurred at the early phase of a spark formation, therefore the final jump or flashover will not be covered in great detail.

A short introduction regarding electrical discharges will be presented. The history on long spark research, complemented with observation of bursts of X-rays from long spark discharges in air will be presented. A short summary about atmospheric lightning and the detection of intense gamma ray bursts up to 40 MeV from satellites and ground level observations will be treated. The research goal is formulated based on the incentives presented. Afterwards, a description of the experimental approach will be given.

1.1 Electrical discharges

An electrical discharge is initiated when the applied electric field exceeds a certain threshold value, the electrical breakdown field (E_k), necessary for a sufficient population of electrons to overcome collisional drag and accelerate to

energies beyond the ionization potential. The ionization rate then must exceed the attachment rate in order to have a net growth in the electron population. A commonly used value for (E_k) at sea level is about $30 \text{ kV}\cdot\text{cm}^{-1}$. When the electric field at the tip of an electrode reaches E_k , conducting streamer filaments begin to emerge from the ionized region and rapidly extend through a normally isolating medium (usually air). These streamers propagate through air and create ionized channels which can ultimately evolve into a spark. Electrical discharge is a common phenomenon in daily life. It varies from a small spark discharge caused by accumulation of electric charge by friction (triboelectric effect) or it can be as impressive as a lightning flash during a thunderstorm.

1.2 History of the problem

The research on electrical discharges developed for many years mainly as an empirical and phenomenological science. An extensive overview on the physics and effects of lightning can be found in [Rak03]. Despite the long history of lightning research, there are still processes that we do not understand yet. The initiation of lightning is still under debate. Thundercloud electric field measurements have only recorded peak values that are an order of magnitude weaker than the dielectric field strength of air [Mar05]. The electric field was measured over a distance of $\approx 50 \text{ cm}$ below a large rising balloon, which influences the results. Researchers increasingly point to the importance of ice particle aggregation for local electric field enhancement. The detection of X-rays from lightning [Moo01, Dwy05a] and later also from laboratory sparks [Dwy05b, Rah08] came as a surprise for researchers. A plausible explanation is bremsstrahlung from energetic electrons. However, these energetic electrons in air can only be produced by the acceleration of lower-energy electrons in the presence of a very high electric field in order to overcome the frictional force, a process called ‘cold runaway’ [Gur61]. Although several theories have been suggested (section 1.2.4), the physical mechanism for this local enhancement of the electric field remains under debate.

1.2.1 Streamers

Streamers are generated by high electric fields and they occur as a precursor to electrical discharges. The foundation for the theory on streamer breakdown, was laid by the work of Raether, Loeb and Meek [Rae39, Loe41]. This theory for the advancement of the streamer mechanism for spark formation was based on the concept of insulated streamer heads emerging from an area of strong electric fields ahead of the streamer head and is independent of the electrodes. This distribution of avalanches ahead of the streamer head have never been

substantiated by further analysis [Ebe06]. Later experimental and theoretical findings have changed some fundamental concepts of this theory, but the basic ideas remained. Numerous applications of streamers are presented in e.g. [Vel00]. The streamer-corona plasma generated in the wire-plate corona reactor presented in Chapter 3 is used for studying the removal of pollutants from gases [Win07]. Recent theoretical and experimental work on the physics of streamer is presented in the PhD theses [Li09a] and [Nij11], respectively.

Experiments applying pulsed high voltage waveforms with tens of nanosecond duration over short inter-electrode distances have revealed traces of X-rays during the streamer propagation [Rep08, Sha11]. This will be discussed in more detail in Chapter 3 together with our own experimental results. Simulations of streamer formation with Monte Carlo models have shown that strong electric field enhancements at the streamer head is capable of producing energetic electrons [Mos06, Li09b, Cha10, Cel11], which could produce X-rays through bremsstrahlung.

Furthermore considerable interest in the streamer/leader process has been stimulated by studies of very long filamentary structures in the upper troposphere, the so-called sprites. This phenomenon, associated with thunderstorms, have been observed from aircrafts [Sen95] and ground [Ina02]. The similarity between streamers and sprites is based on theoretical arguments [Pas03, Ebe10] and confirmed by observations. Results from streamer research used to improve our understanding of sprites is reviewed in [Ebe10]. These high altitude electrical discharges together with the observation of intense bursts of hard radiation have become increasing active areas of study.

1.2.2 Long laboratory Spark discharges

The process of a spark breakdown in air begins when the high voltage electrode is submitted to a fast rising voltage. For positive polarity discharges breakdown is initiated with the formation of corona in the vicinity of the anode tip, where the electric field is concentrated. A corona discharge is a very faint low current discharge. As the voltage increases further long filaments, termed streamers, emerge from this corona region. The streamer zone can grow up to several meters long. In meters long air gaps a streamer channel can evolve into a leader. The leader channel is heated (5000-10000 K) by the total current flowing in from all the streamer branches at the tip. In a long air gap a short circuit occurs after the leader channels have bridged the gap distance. The streamer zone formation at negative polarity requires a higher tip potential. In the case of a negative polarity surge the process of breakdown in air for long gaps is more complicated compared to that of positive polarity and is still not fully understood.

The channel elongation process is discontinuous and propagates in a stepwise manner. The negative leader elongates with every step. Leader elongation is accompanied by repeated streamer outbursts at the leader head. Streak images of the above mentioned processes for positive and negative discharges in air can be found in literature (e.g. [Les81, Gal02, Baz98]).

Experimental study of spark discharges in gaseous gaps has a long history [Mee53, Baz98]. Laboratory discharges in air submitted to impulse voltages of various waveforms have been studied in detail and models have been developed to describe the physical processes during a spark formation, e.g. [Les81, Gal02]. Even sparks up to hundreds of meters long (150-200 m) have been studied. These experimental study into the physics of breakdown in air gaps were of interest for the protection of electrical networks (e.g. determination of risk failure in power transmission systems). The available literature on long laboratory sparks in atmospheric air was mainly focussed on electrical parameters, combined with photographic techniques. However, properties of the spark discharge plasmas remains poorly investigated. Not much attention has been paid to the emission of hard radiation during the spark formation. This phenomenon has been either overlooked or ignored. Bursts of X-rays have been observed in several independent laboratory experiments with a Marx generator in metre-long spark discharges in air [Dwy05b, Rah08, Mar10a].

1.2.3 X/ γ -rays from atmospheric origin

The possibility for influence of cosmic ray secondaries on the lightning discharges was first discussed by Wilson [Wil24]. Later Schonland tried to confirm Wilson's hypothesis in the 1930s in a series of on-ground experiments, but the experimental data obtained were considered statistically insignificant. On the other hand, it was mentioned by Babich [Bab03] that a Russian investigation on laboratory discharges was carried out by Stankevich and Kalinin in 1967 [Sta67] where X-rays appeared in overvoltage gaps under atmospheric conditions. The experiment showed that 'electrons in the initial stage of a spark discharge can gain an amount of energy comparable in magnitude to the applied voltage'. A historical review about these experiments is presented in [Bab03, Ch.2].

It was till the aircraft observations from [Par81, McC85] that showed an increase in radiation flux prior to observed lightning discharges. This is consistent with the qualitative picture proposed by Wilson. Later balloon experiments by *Eack et al* [Eac96], which includes electric field measurements, suggested that the production mechanism for X-rays is related to the storm electric field and not necessarily to the lightning discharge processes.

A direct link between X-rays and lightning was found in the experiments

performed by *Moore et al* [Moo01], where energetic radiation > 1 MeV has been recorded with a NaI(Tl) scintillation detector from several negative cloud-to-ground lightning strikes on a mountain-top. It was suggested that the bursts of energetic radiation originated in the leaders around the tips of the negative stepped leaders where strong electric fields exist. Later observations by *Dwyer et al* [Dwy05a] confirmed this and showed explicitly that the X-rays are produced by the leader stepping process. It was also concluded that the large X-ray pulses observed are not individual MeV γ -rays, but instead are intense bursts of X-rays with energies typically well below 150 keV, occasionally extending up to a few hundred keV. Furthermore, X-rays have also been detected from rocket-triggered lightning [Dwy04]. Balloon measurements by *Marshall et al* [Mar05] have shown that the electric field conditions, volume and field strength, necessary for runaway breakdown can exist prior to a flash in a thunderstorm region.

Bursts of energetic radiation have also been detected from space. These so-called Terrestrial Gamma-ray Flashes (TGFs) have been observed by the Burst and Transient Source Experiment (BATSE) on board the Compton Gamma Ray Observatory (CGRO) satellite [Fis94]. From this first observations it was suggested that these TGFs must originate in the atmosphere at altitudes above at least 30 km in order to escape atmospheric absorption and reach the orbiting detectors. It was also suggested that the origin of the high energy electrons, could be from high altitude electrical discharge above thunderstorm regions. Measurements from the Reuven Ramaty High Energy Solar Spectroscopic Imager (RHESSI) spacecraft indicated that the electron spectrum is extremely hard, enabling the generation of TGFs up to 20 MeV by bremsstrahlung [Smi05]. Recently photons associated with TGF events up to 40 MeV have been detected by the AGILE satellite and the Gamma-Ray Burst Monitor (GBM) on the Fermi Gamma-ray Space Telescope [Mar10b, Bri10]. *Briggs et al* also reported on the detection of electrons and positrons as a result of pair production next to the energetic photons [Bri11].

These observations suggested that TGFs occur relatively high in the atmosphere and are probably not from the same origin as X- or gamma-rays seen on the ground [Smi05]. However, later Monte Carlo simulations [Car07, Gje10] from TGFs detected by BATSE have revealed a lower production altitude (14-22 km) after taking into account the dead time loss from BATSE instrument [Gre08]. These values for production altitude are close to the values obtained from simulations from RHESSI detected TGFs [Dwy05c, Haz09]. Analysis of TGFs detected by RHESSI and the lightning processes observed by the Los Alamos Sferic Array (LASA) has pointed to an estimated height for the TGF-related lightning pulses to be in the range of 10.5-14.1 km [Sha10].

1.2.4 Runaway breakdown

For a long time the mechanism for electrical breakdown was dominated by the concept of ionizing gas by applying a sufficiently strong electric field. In this process fast electrons in the tail of the distribution function have gained enough energy to ionize matter and thus are able to generate new free electrons. In the presence of this same electric field these newly freed electrons can in turn free more electrons, comparable with an avalanche effect. This process is called the ‘conventional breakdown’ (CB) and has been studied extensively in the laboratory [Loe39, Rae64, Rai91, Baz98]. Characteristic electron energies in this process responsible for ionization are 10-20 eV, while recombination mostly takes place at low energies. For this reason, mean electron energy $\bar{\epsilon}$ considered here does not normally exceed several eV’s.

The second mechanism is a relatively new one, the so-called ‘runaway breakdown’ (RB) and was first advanced by *Gurevich et al* [Gur92] and involves an avalanche of relativistic electrons that are aligned by the applied field to form an electron beam. Unlike conventional breakdown, the runaway breakdown does not require a high electric field. The critical electric field (E_c) to initiate runaway breakdown is one tenth of the conventional threshold field under the same pressure conditions. Instead, it requires the presence of energetic seed electrons with energy in excess of tens of keV in the high electric field region in order to get started. Such energetic electrons are often present in the atmosphere as secondaries generated by cosmic rays [Tak11]. In the original concept seed electrons are provided by cosmic-rays, however, recently alternative source of relativistic seed electrons are proposed. A process called ‘positive feedback’ [Dwy03, Dwy08, Bab05] is a candidate theory for providing the necessary seed electrons if the total field region is large enough (with $U > 100$ MV). Another candidate theory is the generation of seed electrons in streamer and leader heads [Mos06, Li09b, Cha10, Cel11]. Detailed Monte Carlo simulations of the cosmic ray secondary flux distributions relevant to relativistic runaway electron avalanche (RREA) seedings, including statistical fluctuations, are presented in [Car08]. Simulations of the RREA initiation process and effective seeding efficiencies for various seeding geometries, particle types, and energies are also included.

1.3 Motivation and scope of this study

Electrical discharges in air were thought to be conventional discharges in which the electron energy is limited to a few tens of electronvolt due to the many collisions. Indeed many discharges and arcs can be described this way in respect of electric fields or voltages. However, Wilson already suggested in 1924 that

‘extremely penetrating corpuscular radiation’ could be associated with lightning [Wil24]. It is only till recent that this topic has become a major subject of study. Observations of X-ray bursts from laboratory sparks have opened a new door the study of processes responsible for this high energetic radiation phenomenon. The possibility of high energy processes involved in the development of a long spark discharge in air has only been demonstrated, but an adequate model to describe this phenomenon is still not available. The conditions for X-ray emission are still poorly understood. There is not much experimental data available to begin with. Laboratory research has largely been focussed on external spark characteristics, such as discharge current, breakdown voltage, leader propagation, etc. Relevant data on plasma parameters such as the electric field near the ionization front in the streamer head is only available from theory, but has never been verified experimentally. An important reason is the complexity of the discharge phenomenon. Streamers/leaders are fast processes and their paths are unpredictable, especially in long spark discharges. Direct measurement of electric field near the streamer/leader head is therefore very challenging and has not been done before. One must also keep a safe distance in order to prevent unwanted flashovers. Experimental results [Sta67] have approximated the duration of a single X-ray flash to be less than 1 ns. This means that fast X-ray detectors in combination with good energy resolution is needed, which only became available in the last decades. Streamer models including the generation of energetic particle have emerged and are being improved for accuracy. Laboratory data, such as obtained in this study, could be used to verify these simulation models.

1.4 Research goals

The recent detection of X-ray bursts from laboratory sparks in air has puzzled scientist’s understanding of the discharge mechanism. It appears that there are unknown processes involved that could lead to the production of hard radiation. From a scientific point of view it is challenging to study this new phenomenon and we try to gain more insight into these processes by collecting experimental data during a long spark discharge. We measure the electrical parameters during a surge simultaneously with the bursts of high energetic emissions (an aspect that has been ignored in decades of laboratory experiments on long sparks in air) and attempt to link these emissions with processes during the surge (e.g. when, where and what the energies of the photons produced during the spark formation are).

1.5 Scientific approach

For the study of X-ray burst emission, it is necessary to monitor the electrical parameters during the discharge, combined with proper X-ray measurements. The investigation in this new phenomenon is experimental in nature. Before starting with the experiments, good considerations must be taken with respect to the electromagnetic disturbances produced during the spark formation. The measurement equipment together with the cables need to be shielded against electromagnetic interference and the noise level should be reduced to an acceptable level. This means that all equipment must be placed inside a grounded metal shielded cabinet, a so-called an EMC¹ cabinet, and all the cables through this cabinet must be properly connected or filtered if required.

First, the presence of X-rays must be verified in our own high voltage laboratory. A twelve stage Marx generator was available to deliver the necessary high voltage for air breakdown. A NaI(Tl) scintillation detector from Radboud University Nijmegen was available for these preliminary experiments. Once the hard radiation during the spark formation is detected, the effects of surge polarity and peak voltage amplitude on X-ray emission can be studied. The detection of X-ray is not efficient if the detector is placed too far from the spark, but getting too close to the spark can result in a direct flashover towards or induce streamers on the sharp edges of the EMC cabinet. Experiments with different electrode positions, varying gap lengths and detector distances have been carried out.

For the detection of X-rays a fast detector with good energy resolution and preferably with a large detecting surface is needed. From preliminary experiments it became clear that the NaI(Tl)'s time response on energetic photons was not adequate; traces of pile-up of X-ray pulses were noticeable. A faster X-ray detector with an energy resolution at least as good as or even better than that of the NaI(Tl) detector is needed. A fast BaF₂ scintillation detector was used in an attempt to resolve the pile-up problem. Simultaneously a LaBr₃(Ce⁺) scintillation detector was also included in the experiments. At that time, this was a new type of scintillation material developed at the Interfaculty Reactor Institute (IRI) in Delft and commercialized by Saint-Gobain. Characteristics of this material are elaborated in Chapter 2. During the course of the experimental investigation an opportunity arose to conduct experiments using a test CZT semiconductor X-ray detector from the Atmosphere-Space Interaction Monitor (ASIM) project.

Measurements of the current formation from both electrodes are required in order to monitor the development of the spark discharge. These measurements

¹Electro Magnetic Compatibility

time synchronized with the X-ray detector responses, reveals the timing of the X-ray emissions with respect to the spark formation and also give a rough indication of where the X-ray bursts are generated. For measuring the current on the high voltage electrode an optical data transmission system had to be constructed.

Results obtained with the $\text{LaBr}_3(\text{Ce}^+)$ detector showed that the relation between the energy of the X-ray quanta and the signal from the scintillation detector is not straight forward. Although large X-ray signals were detected, it remains difficult to imagine that quanta with energy larger than $q \cdot V_{max}$ could be produced. The X-ray detector's response to energetic electrons as well as to energetic photons makes interpreting the signals more complicated. Absorption measurements should point out what order of magnitude the energies of these quanta are.

Validation of the correct X-ray detector response on the quantum energies recorded is required to assure that the detector or photomultiplier tube is not saturated during the measurements. Small radioactive calibration sources (^{241}Am , ^{137}Cs and ^{60}Co) with known emitting characteristics are suitable for this.

By critically analyzing the measurements regarding the electrical parameters, combined with X-ray detector data and earlier laboratory studies from literature, more insight was gained in the conditions leading to the emission of bursts of hard radiation.

An additional experiment with a streamer-corona-reactor configuration by applying fast pulsed high voltage waveforms with tens of nanoseconds rise time was performed in order to verify the streamer phase as a new source for X-ray production.

1.6 Structure of the thesis

The background research on high energy phenomenon in electrical discharges is presented above. An introduction to the high energy phenomenon is given. An overview on laboratory spark discharges and atmospheric lightning research was presented above. In addition, the theory of runaway electrons (proposed by Gurevich) has been presented.

Chapter 2 presents characteristics of the various X-ray scintillation detectors ($\text{NaI}(\text{Tl})$, BaF_2 and $\text{LaBr}_3(\text{Ce}^+)$) and one semiconductor detector (CZT) used during the experiments. Performance of each detector is discussed based on the detector's response on energetic emissions during the experiments. Investigation in the linearity of the $\text{LaBr}_3(\text{Ce}^+)$ scintillation detector is included.

Chapter 3 presents X-ray measurements from a wire-plate corona reactor

configuration, where only short streamers are produced. Since the fast streamer discharges are highly reproducible, we can focus more accurately on the timing of X-ray emission.

In Chapter 4 the experimental set-up and the experimental procedure for investigating long spark discharges are presented, followed by the discussion of the results obtained with various scintillation detectors.

Chapter 5 presents experimental results obtained with the addition of the current measurement on the high voltage electrode. A more complete picture of the spark development is obtained by monitoring the current on both electrodes. With this additional measurement it was possible to link the X-ray emission with the streamers more accurately. A strong correlation between X-ray bursts and negative streamers was observed.

In Chapter 6 important conclusions are summarized and recommendations for future work are proposed.

CHAPTER 2

X-RAY DETECTORS

In this chapter, the performance of three scintillation detectors and the Cadmium Zinc Telluride (CZT) semiconductor X-ray detector used in the experiments are presented. A short introduction to scintillation detector properties is given along with a discussion about the suitability of each one of these X-ray detectors for the experiments. We started our investigation with the NaI(Tl) detector. This detector was soon superseded by a BaF₂ and a LaBr₃(Ce⁺) scintillation detector because of their shorter decay time and superior energy resolution respectively. Because most of the X-ray detection have been performed with the LaBr₃(Ce⁺) scintillation detector, an investigation of this detector's linearity had to be included in this chapter. Finally, preliminary results obtained with a small test CZT semiconductor detector, developed for the ASIM project, is also presented and discussed in this chapter.

2.1 Introduction

In general X-ray detectors can be divided in three types:

- Gas-filled detectors; high-energy rays or particles ionize the gas when colliding with gas atoms.
- Scintillation detectors; the absorption of radiation produces light flashes in the scintillation crystal.
- Semiconductor detectors; electron-hole pairs are produced when high-energy rays or particles cross the detector material.

The efficiency in which the detector measures a particular type of incident radiation depends on the efficiency in the charge created (electron-ion or electron-hole pairs) by this radiation type along its tracks within the detector material.

2.2 Scintillation detectors

2.2.1 Introduction to scintillation detectors

Today, scintillation detectors are used in a wide array of applications including fundamental research in particle and nuclear physics, oil exploration, field spectrometry, container and baggage scanning, health physics, space physics, industrial gauging and medical diagnostics and therapy. The scintillation material may be organic or inorganic; the latter is more common and is also used in our experiments.

The most important application of scintillation detectors is photon (X- and γ -ray) spectroscopy. The purpose of a scintillation detector is to produce a large light output in the visible range. When for example an incident X- or gamma quantum interacts with the scintillation material, the produced secondary charged particle deposits its energy in this material. In a pure inorganic scintillation crystal, the return of an electron to the valence band with the emission of a photon is an inefficient process. Furthermore, the emitted photons are usually too high in energy to lie in the range of wavelengths to which the photomultiplier tube (PMT) is sensitive to. Small amount of impurities (called activators) are added to the scintillators to enhance the emission of visible photons. Four interaction mechanisms can occur when a photon interacts with matter.

- Photoelectric absorption: An incident photon removes an electron from its nucleus; part of the photon energy is needed to liberate the electron, the rest of the energy is transferred to the kinetic energy of the electron.
- Compton scattering: The incident photon transfers part of the energy to an electron and the recoil (or Compton) electron is emitted after scattering.
- Rayleigh scattering: When the incident photon is scattered by the atom and changes its direction, the target atom recoils to conserve momentums before and after scattering. Since the atomic mass is relatively heavy, the recoil energy of the atom is negligible and the photon changes its direction only and retains the same energy after scattering; no energy is transferred.
- Pair production: The incident photon energy can be converted to the creation of an electron-positron pair. This only occurs if the photon energy

is twice the electron rest mass of 511 keV (above the threshold of $2m_e c^2 \approx 1.02$ MeV).

The probability associated with each of these kinds of interaction depends on the energy of the incident photon, the scattering angle and the atomic number of the absorber (the scintillation material). For the experiments considered here, photoelectric absorption and to a lesser extent also Compton scattering are more likely than the other types of scattering. Rayleigh scattering is not involved in the detection process, since no energy is transferred.

At low energy, in high atomic number materials, photoelectric absorption is the main effect. This is also the most desirable interaction in the scintillation crystals. The kinetic energy of the photoelectron E_e liberated by the photoelectric effect is given by

$$E_e = E_\gamma - E_b$$

where E_γ ($= h\nu = h\lambda/c$) is the incident photon energy and E_b the electron binding energy. The vacancy in the electron shell is quickly filled by electron rearrangement; electrons from higher energy levels fill the vacancy. Assuming the binding energy is absorbed, a constant fraction of the radiation energy is converted into light. This effect is important when determining the actual energy of the impinging X- or γ -ray photons. At intermediate energies in low atomic number materials the dominant interaction is Compton scattering. And at very high energies pair production is the main mechanism by which photons can be detected, as mentioned above.

During our experimental study mostly scintillator detectors were used. Scintillator materials operate by converting energy lost by incoming ionized radiation into flashes of visible light. A review on scintillator detectors for X-rays is presented in [Nik06]. The scintillation light is emitted isotropically; so the scintillator is typically surrounded with reflective material to minimize the loss of light and then is optically coupled to a sensitive light detector such as a photomultiplier tube or a photodiode. Each scintillation material has a characteristic emission spectrum. The spectrum of this emission depends on the type of excitation (photons or particles). The emission spectrum is of importance when choosing the optimum readout device (PMT or photodiode).

All the scintillation detectors used in the experiments have a PMT integrated for optimal light to electrical signal conversion. For the $\text{LaBr}_3(\text{Ce}^+)$ scintillation detector the entire assembly is mounted in a metal housing with μ -metal shielding to protect the PMT against magnetic fields. The PMT is a vacuum tube which consists of a photocathode, an electron multiplier (composed of several dynodes) and the output electrode (the anode). A scintillation light photon may interact

in the photocathode at the entry window of the PMT to eject a low-energy photoelectron (≈ 1 eV). The electron then undergoes the following processes:

1. acceleration by electric field between dynodes
2. collision with dynode at about 100 eV (assuming 100 V between dynodes)
3. more secondary electrons upon collision with dynode

A chain of multiple dynode stages increases the electron flux further and can create very large electron gains (by a factor of 10^5 or more). The result is an electrical pulse signal at the anode, large enough for further processing. In this manner the photomultiplier tube enables individual photon detection provided the incident flux of light is not too high. In order to translate this electrical signal back to the energy of the absorbed radiation, the scintillation material and PMT must not saturate (as will be discussed in more detail below in section 2.2.4.1). A value for the energy of the absorbed radiation can be obtained with a calibration source; the 662 keV γ 's from a ^{137}Cs source is commonly used.

A large number of different scintillation crystals exist for a variety of applications. The maximum size of a scintillation crystal varies very much between different materials. This has to do with crystal growing physics related to the physical properties of the material. For NaI(Tl) crystals relatively large diameters can be manufactured, whereas for $\text{LaBr}_3(\text{Ce}^+)$ it is more difficult to grow large scintillation crystals. The anisotropic thermal expansion due to the hexagonal crystal structure of this crystal causes internal stresses as the crystal cools after growth, careful procedures are required to prevent cracking of large crystals. Nowadays larger diameters up to 3 inches are commercially available. Important requirements for the scintillation crystals used in X- or γ -ray detection include:

- High light output; plays a key role in the accurate determination of the energy of the radiation.
- High stopping efficiency; a material with a high density and high Z is needed for efficient detection of X- or γ -rays.
- Fast response; the decay time is important for fast counting and/or timing applications.
- Good proportionality; the conversion factor between the energy deposited in a scintillator material and the number of visible photons produced (scintillation light yield) should ideally be proportional. Non-proportionality has a deteriorating effect on the energy resolution [Dor95, Kho11].

- Minimal afterglow; the fraction of scintillation light still present for a certain time after a X-ray excitation should be as low as possible in order to detect fast changes in transmitted intensity of X-rays.
- Low fabrication cost and subject to manufacture in large size; unfortunately the production process of $\text{LaBr}_3(\text{Ce}^+)$ (or patent protection) is still very costly which makes it more expensive compared to other scintillation detectors.

It is clear that none of the presently known commercially available scintillator possesses all of the above mentioned (ideal) characteristics, and there is a continued interest in the search for new scintillators with enhanced performance. The choice of a certain scintillation crystal for radiation detection depends on the application. The light output is a strong function of the type of incident particle or photon and of its energy, which therefore strongly influences the type of scintillation material to be used for a particular application.

The light pulse of a scintillation detector is characterized by a fast rise time (limited by the PMT) and a $1/e$ decay time. The decay time of a scintillator is often defined by the time after which the intensity of the light pulse has returned to $1/e$ of its maximum value.

An important aspect of an X-ray detector is the ability to discriminate between photons with slightly different energy. This quality is characterized by the energy resolution which is defined as the ratio of the full width at half maximum (FWHM) of the (full-energy) photopeak to the peak position, usually expressed in %. This peak represents the pulses that arise from the full-energy, photoelectric interactions in the detection medium. A high energy resolution (small FWHM) means a good ability to discriminate between photon energies. Next to the γ -ray energy, the energy resolution is influenced by:

- The light output of the scintillator
- The size of the scintillator
- Photomultiplier characteristics (quantum efficiency and photocathode homogeneity)

The width of the photopeak is significantly broadened by the statistical fluctuation in the number of electron-ion pairs produced by the photoelectron in the scintillation medium, the variation in the number of electrons liberated from the PMT photocathode and from the statistical variations from the emission of secondary electrons from the dynodes in the PMT. All these effects add to the deterioration of the energy resolution of a scintillation detector.

The subsequent sections present results obtained with three different types of scintillation detectors and the Cadmium Zinc Telluride (CZT) semiconductor X-ray detector. The suitability of these detectors for the experiments is considered based on their results. Several characteristics of the scintillation detectors are collected in Table 4.1.

2.2.2 NaI(Tl) scintillation detector

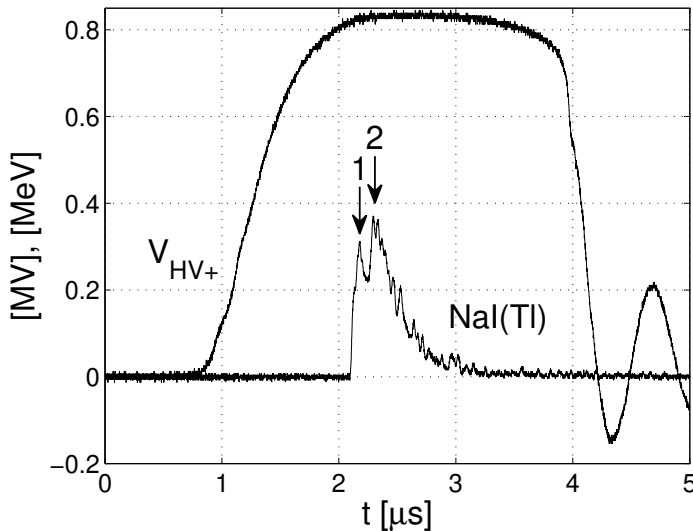


Figure 2.1: An example of indication for pile-up in a NaI(Tl) detector's response (shown inverted) during a positive high voltage surge V_{H+} . It appears that a second X-ray peak at $t = 2.2 \mu\text{s}$ is superimposed on the slope of the first one.

NaI(Tl), first produced in the early 1950s, is the most widely used scintillation material in radiation detection. From the commercially available scintillators, NaI(Tl) has one of the highest light yield and it is available in a wide variety of sizes and geometries (large collecting area possible). Modern detector performances are often compared with NaI(Tl). The crystals are usually coupled with a photomultiplier tube. Since sodium iodide is hygroscopic, it has to be hermetically sealed. The energy resolution for 662 keV γ 's absorbed in small NaI(Tl) detectors is 6 to 7%. At low energies, e.g. at 5.9 keV, the energy resolution drops dramatically to around 45%. The deviation in scintillation light yield gets larger for low energies [Dor95]. At these low energies, surface treatment of the scintillation crystal strongly influences the resolution. *Kaiser et al* [Kai62]

observed that the response of NaI(Tl) at energies below 20 keV is sensitive to the surface treatment of the crystal, whereas at higher energies it is insensitive to the treatment. This surface effect might be caused by one or more of the following processes:

- Additional quenching of the fluorescence near the crystal surface, due to chemical deterioration or other modification of the surface layer.
- Surface escape of light pulses, emitted during the scintillation process, which would otherwise be sent to the cathode of the PMT.

The few X-ray bursts recorded with the NaI(Tl) scintillation detector shows traces of pile-up in the detector's response. An example is shown in Figure 2.1, where the X-ray pulse signal from the NaI(Tl) detector is shown inverted. A second X-ray pulse (at $t = 2.2 \mu\text{s}$) is superimposed on the decay flank of the first pulse (starting at $t = 2.1 \mu\text{s}$). This recording shows that a faster X-ray detector is needed.

2.2.3 BaF₂ scintillation detector

A few measurements have been performed with a BaF₂ scintillation detector because of its good time resolutions. BaF₂ crystals are characterized by a very fast scintillation emission with a decay time of 800 ps at 220 nm and a slow component in the wavelength range between 250 and 400 nm with an emission time of 620 ns. The existence of the fast component makes it possible to use such crystals for fast timing measurements where a sub-nanosecond time resolution is required. Typical time resolutions are 150 ps at 1 MeV. In our experiments we only considered the fast component for timing of X-ray bursts onset, as will be discussed in more detail in Chapter 4. A disadvantage of BaF₂ is the relatively low light yield relative to NaI(Tl) (5% for the fast component and 16% for the slow component) [Scib]. The energy resolution is $< 12\%$ at 662 keV photons, with a fast/slow ratio > 10 [Scia]. This energy resolution is inferior to the 6 to 7% of NaI(Tl).

It is worth to mention that according to [Dor93] the value for light yield for BaF₂ has been overestimated due to the higher quantum efficiency of the XP2020Q PMT (same as in our detector) than specified by the manufactures with more than a factor of two. The reported photon yield for pure BaF₂ at room temperature obtained using 662 keV γ 's is 1400 ± 80 photons/MeV whereas a value of 2000 photons/MeV is often reported in literature for the fast component. This may have consequences for the energy resolution posted in the datasheet.

But since we only use the BaF_2 scintillation detector for timing purpose, this aspect can be ignored.

In experiments where the BaF_2 detector was placed parallel to the $\text{LaBr}_3(\text{Ce}^+)$ detector, we only recorded one BaF_2 signal at the onset of the broader $\text{LaBr}_3(\text{Ce}^+)$ pulse signal and not a pulse train of the fast component of BaF_2 . The waveforms shown in Figures 2.2 indicate that the BaF_2 detector is not capable of resolving the pile-up signals seen with $\text{NaI}(\text{Tl})$ and $\text{LaBr}_3(\text{Ce}^+)$. The large and broadened X-ray pulse with an energy amplitude of 6.3 MeV cannot be from a single photon. However, the BaF_2 detector's fast decay time is useful for the timing of X-ray bursts occurrences in the fast streamer front.

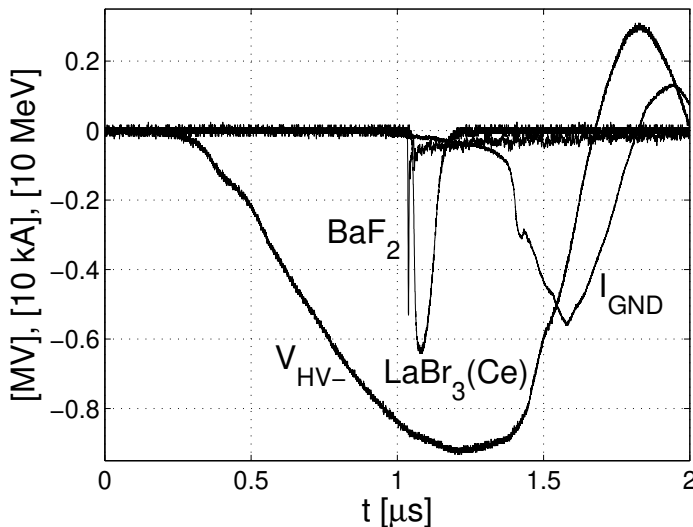


Figure 2.2: BaF_2 and $\text{LaBr}_3(\text{Ce}^+)$ detector's response during a negative high voltage surge $V_{\text{HV-}}$. Despite the broadening of the $\text{LaBr}_3(\text{Ce}^+)$ waveform with 6.3 MeV energy amplitude, no multi-bursts could be recorded with the faster BaF_2 detector. I_{GND} is the current measured at the grounded electrode.

2.2.4 $\text{LaBr}_3(\text{Ce}^+)$ scintillation detector

Not long before the start of our experimental study the $\text{LaBr}_3(\text{Ce}^+)$ scintillation detector [Loe01, Loe02] became commercially available. This scintillator has attractive scintillation properties such as a very high light output ($> 61,000 \pm 5000$ photons/MeV), a fast principle decay constant (30 ± 5 ns) and good energy resolution (about $3.8 \pm 0.4\%$ at 662 keV). The scintillation mechanism

of this material is further reviewed in [Dor05]. Properties of the $\text{LaBr}_3(\text{Ce}^+)$ scintillation detector has been investigated in [Ilt06] where count rates up to 1.8 Mcps (limited by the set-up) have been achieved. Based on these excellent properties, we decided to use the $\text{LaBr}_3(\text{Ce}^+)$ scintillation detector for the X-ray detection during long spark formation. Indeed, multiple X-ray pulses can clearly be distinguished in the data obtained with $\text{LaBr}_3(\text{Ce}^+)$. Figure 2.3 shows a multi-burst detection with the second pulse on the decay shoulder of the first pulse. Figure 2.4 shows two well separated X-ray burst detections. Remarkably such multi-bursts measurement have not been seen with the BaF_2 detector. Considering the almost equal response time window of BaF_2 and $\text{LaBr}_3(\text{Ce}^+)$ on incident radiation (with coincidence timing resolution of 240 ps FWHM and 260 ps FWHM respectively [Sha03]) and the superior decay time of BaF_2 's fast component, one would expect to record more multi-bursts with this scintillation detector. Also according to [Kum09], the detection efficiencies of $\text{LaBr}_3(\text{Ce}^+)$ and BaF_2 are comparable over a wide range of gamma energy from 500 keV to 50 MeV. The lack of multi-bursts detection with BaF_2 for various set-up positions shows that $\text{LaBr}_3(\text{Ce}^+)$ is more suitable for our experiments, mainly due to the much better energy resolution.

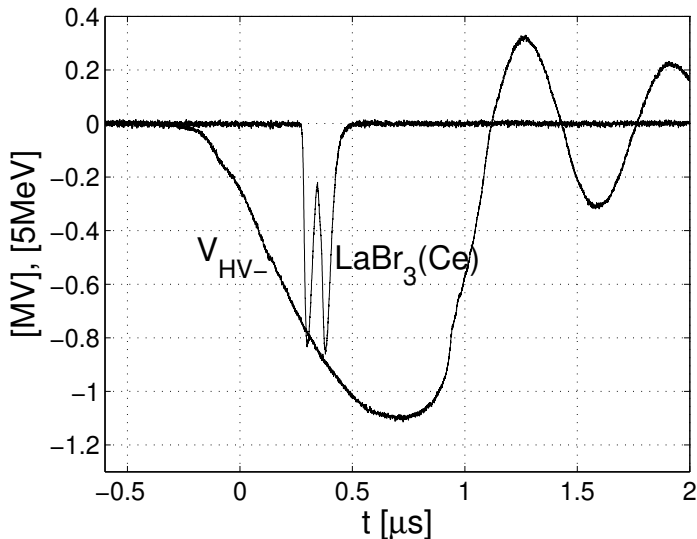


Figure 2.3: Multi-bursts detection recorded with a $\text{LaBr}_3(\text{Ce}^+)$ detector during a negative high voltage surge V_{HV-} . Two energy amplitudes of 4.1 and 4.2 MeV was recorded.

Unfortunately, $\text{LaBr}_3(\text{Ce}^+)$ has a few drawbacks due to internal radioactivity

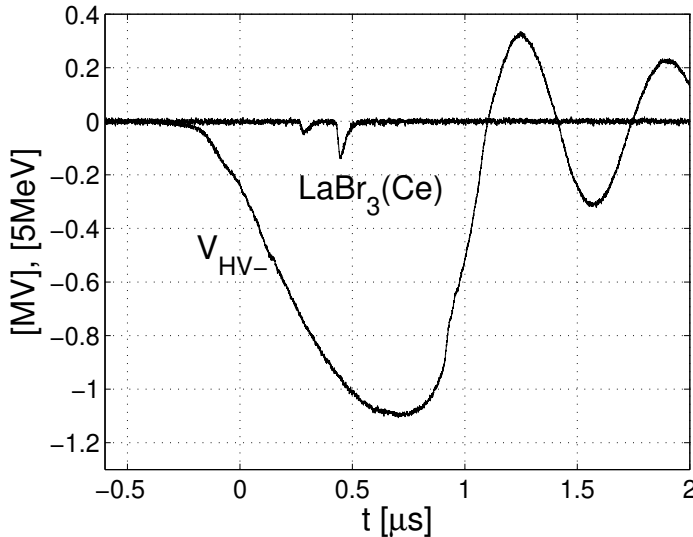


Figure 2.4: Well time separated multi-bursts detection recorded with a $\text{LaBr}_3(\text{Ce}^+)$ detector during a negative high voltage surge V_{H-} .

and a sharp drop in proportionality below 20 keV. The latter one results in a poorer energy resolution with respect to $\text{NaI}(\text{Tl})$ for energies below 100 keV. Internal radioactivity is caused by the presence of ^{138}La and ^{227}Ac . Actinium has similar chemical properties as lanthanum and other lanthanides, and therefore these elements are difficult to separate when extracting from uranium ores. However, the ^{227}Ac impurity has been significantly reduced with improved manufacturing experience in growing the crystal. The isotope ^{138}La makes up 0.09% of the naturally occurring lanthanum, has approximately a $1.06 \cdot 10^{11}$ year half-life and emits 788.7 keV γ -ray from beta decay (34 percent, 255 keV endpoint energy) and 1435.8 keV γ -ray from electron capture (66 percent, 302 keV endpoint energy) in its decay to stable ^{138}Ba [Mil07]. ^{227}Ac has a 21.77 year half-life and occurs naturally as part of the ^{235}U decay series. These gamma rays are evident in the background spectrum, but have little chance to show up in the experimental measurements. This can be demonstrated in the following estimation for the ^{138}La isotope in the scintillation material: The size of the scintillation crystal with $5.29 \text{ g}\cdot\text{cm}^{-3}$ density is 43.44 cm^3 (1.5" diameter by 1.5" long). The half-life of $^{138}\text{La} \approx 3.34 \cdot 10^{18} \text{ s}$. The molar mass (M_u) of $\text{LaBr}_3 = 137.91 + 3 \times 79.90 = 377.61 \text{ g}\cdot\text{mol}^{-1}$. The number of atoms per $\text{cm}^3 = (5.29/377.61) \times 6.02 \cdot 10^{23} = 8.44 \cdot 10^{21}$. For the crystal volume this value will be $43.44 \times 8.44 \cdot 10^{21} = 3.66 \cdot 10^{23}$ atoms. Taking into account the 0.09% naturally occurring of the ^{138}La isotope

it will take about $3.34 \cdot 10^{18} / (0.0009 \times 3.66 \cdot 10^{23}) = 10.13$ ms for a gamma to be released. Within the $2.5 \mu\text{s}$ measuring time duration (taken from Figure 2.3) the chance to detect a gamma from the ^{138}La decay is $\approx 2.47 \cdot 10^{-4}$. This value is close to the intrinsic background of about $1\text{-}2 \text{ count}\cdot\text{cm}^{-3}\cdot\text{s}^{-1}$ postulated in [Kno10, p.251]. For 43.44 cm^3 this would result in a chance of $\approx 2.25 \cdot 10^{-4}$ for detecting the intrinsic background of $\text{LaBr}_3(\text{Ce}^+)$ within a $2.5 \mu\text{s}$ measuring time window. This means that only for low count rate radiation measurements just above the background the intrinsic radioactivity will be a hindrance.

2.2.4.1 Linearity of the $\text{LaBr}_3(\text{Ce}^+)$ scintillation detector

An ideal X-ray detector would be perfectly linear, i.e. its output pulse height should be exactly proportional to the deposited energy in its sensitive region. In reality, deviation from linearity is always present due to the statistical fluctuation in the processes mentioned in section 2.2.1). In order to obtain meaningful values for the radiation energies detected with the scintillation detector, one must be certain that the detector's response on the incident radiation is linear. A saturated detector response would mean that the amplitude of the pulse signal is limited by material properties and does not represent the energy detected correctly (the actual value is higher). This deviation from linearity is dominated by two factors:

1. Non linearity in the $\text{LaBr}_3(\text{Ce}^+)$ scintillator crystal.
2. Photocathode saturation.
3. Saturation in the PMT gain.

The first cause is less likely for the single photon energy range we are studying (only up to several hundred keV's). With $q \cdot V_{max}$ around 1 MeV as determined by the setup. High energy γ -ray measurements in the 700 keV to 17.6 MeV range have shown a linear response up to 10 MeV [Cie09]. The proportionality of response of $\text{LaBr}_3(\text{Ce}^+)$ (as a function of energy) in light yield over the energy range from 60 keV to 1275 keV is about 6%, which is substantially better than that for many established scintillators [Sha03]. Photocathode saturation can occur if photocathode current exceeds a particular value causing a potential drop across its surface. This potential drop modifies the electric field between the photocathode and the first dynode, deteriorating the collection of photoelectrons. The current limit depends on the actual photocathode resistivity, which depends on the particular photocathode material and operational temperature [Qua11]. Once a particular PMT photocathode is chosen, saturation cannot be avoided, but only mitigated in its effects by keeping a high bias between the photocathode

and the first dynode [Ham]. This is simply achieved by increasing the resistor values in the photocathode grid first dynode part of the chain. Saturation in the PMT is more likely, since $\text{LaBr}_3(\text{Ce}^+)$ produces a very large number of light photons in a very short period of time. This produces a high instantaneous current in the PMT, causing the voltage to drop between the dynodes. The result is a deviation from linearity in the energy response [Dor04]. When the PMT reaches to saturation, peaks are widened. The amplitude is mostly limited by space charge effect between dynodes which can modify the electron trajectories and deteriorate the multiplication process and response proportionality [Ham]. The most straightforward way to avoid PMT gain nonlinearity is to reduce the gain by decreasing the bias voltage over the PMT or by reducing the number of dynode stages. A tapered divider (to compensate for the space charge effect caused by an increase in the electron density between the electrodes) can also improve the pulse linearity. A detailed investigation of PMT saturation and alternative solutions to reduce the PMT gain and/or number of active dynode stages is presented in [Qua11].

The linearity of the $\text{LaBr}_3(\text{Ce}^+)$ scintillation detector has been investigated. The BrillanCe-380, Saint-Gobain Crystals trade name for $\text{LaBr}_3(\text{Ce}^+)$, was delivered with a Hamamatsu R6231-100-01 PMT consisting of 8 dynodes. This low number of dynode stage matches better with the high light output of the crystal. We measured an energy resolution of approximately 3.3%, but better energy resolution (less than 3%) have been reported. The result of our linearity analysis is shown in Figure 2.5. The measurements were done with several radioactive sources: ^{241}Am (59.5 keV), ^{137}Cs (662 keV) and ^{60}Co (1173 keV, 1332 keV and 2505 keV). The sources all have a low count rate, which means that pile-up during the calibration can be excluded. These sources were placed at a distance of 8 cm from the front face of the $\text{LaBr}_3(\text{Ce}^+)$ detector. This reduces the chance of escaping γ 's. The 2505 keV was obtained by capturing the sum peak from ^{60}Co source. For this measurement the ^{60}Co source was put against the detector front in order to increase the chance for double absorption. To reduce the fluctuation in the signal, an average over 5000 samples was taken for the 59.5 keV and the 662 keV and an average over 3000 samples was taken for the rest (the ^{60}Co source was less active). The measurements for these 5 energies have been carried out for increasing values of the PMT bias voltage, starting at 568 V and moving up to 1000 V. From Figure 2.5 it can be seen that linearity is excellent up to 700 V bias voltage over the full energy range considered. At 750 V good linearity holds up to 1332 keV, a deviation from linearity of approximately 8.6% takes place only at 2505 keV. Deviation from linearity increases with increasing bias voltage, as expected. At 1000 V PMT bias voltage the deviation from linearity is approximately 11.3% at 1332 keV.

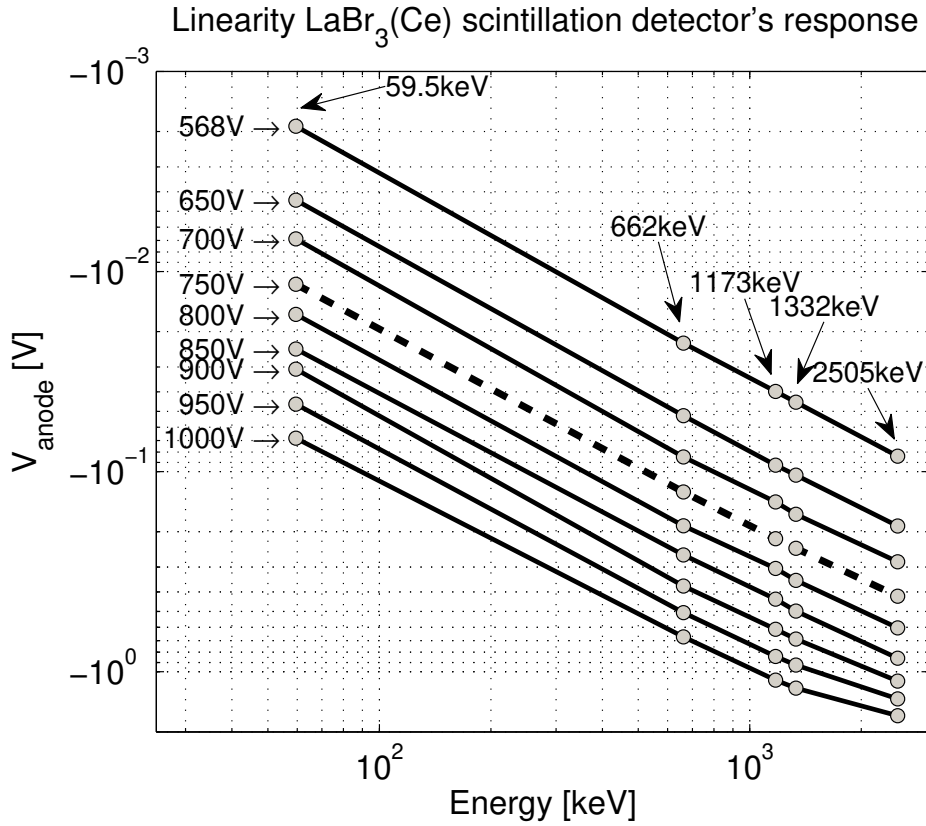


Figure 2.5: $\text{LaBr}_3(\text{Ce}^+)$ scintillation detector's response for photon energies from ^{241}Am (59.5 keV), ^{137}Cs (662 keV) and ^{60}Co (1173 keV, 1332 keV and 2505 keV from the sum peak). Good linearity is noticeable for low (up to 850 V) PMT bias voltage.

From absorption measurements (presented in Chapter 4) we expect single photon energies up to a few hundred keV's maximal to be produced during the spark formation. The result presented here indicates that we can assume the $\text{LaBr}_3(\text{Ce}^+)$ scintillation detector's response to be linear in our experimental conditions, especially considering that a bias voltage of 750 V has been used throughout the experiments. This means that saturation in the X-ray pulses recorded due to single photon detection can be excluded in our experimental condition. However, saturation cannot be excluded when pulse pile-up occur and the data should be fitted in order to obtain information about the total energy deposited in the detector (the fit procedure is described in section 4.2.1). The multiple nearly overlapping peaks occasionally detected (with detector at adequate distant from high voltage electrode configuration) can be ascribed to

pile-up of lesser energetic photons due to inadequate detector's time response, but does not necessarily lead to detector saturation.

2.3 Cadmium Zinc Telluride semiconductor detector

A preliminary experiment with a small ($10\text{mm}\times 10\text{mm}\times 2.5\text{mm}$) test pixelated CZT drift strip detector, developed at DTU Space [Kuv10], was performed in the high voltage laboratory at Eindhoven University of Technology in order to test this detector's performance for the detection of hard radiation produced during a long spark discharge. This type of detector will be used for the detection of high energetic phenomenon triggered by lightning in the upcoming high energy astrophysics mission, part of the Atmosphere-Space Interaction Monitor (ASIM) project [Bud09]. ASIM is a number of specially designed cameras for the International Space Station that will observe the Earth's atmosphere. It will give new insights into climate processes that can help improve climate models [ASI]. Mounted on the ISS external facilities on the Columbus module, ASIM will study giant electrical discharges (lightning) in the high-altitude atmosphere above thunderstorms.

2.3.1 Introduction to semiconductor detector

Semiconductor detectors are fundamentally different from scintillation detectors. They rely on the sensitivity to the charge carriers (electrons and holes) generated in semiconductors by energy deposited by gamma-ray photons, whereas scintillation detectors convert energy lost by incoming ionizing radiation into pulses of visible light. Cadmium Zinc Telluride (CZT) is one of the most promising materials. Unlike some other materials CZT is a room temperature semiconductor that directly converts X- or gamma-ray photons into electrons. Additional advantages include high sensitivity for X- and gamma-rays due to the high atomic numbers of Cd and Te, and an energy resolution [Kuv05] that outperforms scintillation-based detectors. A drawback of the CZT detector is the ineffective charge collection of holes within the detector due to its short mean drift length (in the order of a few hundred microns). Therefore the holes are severely trapped within the detector. As a consequence the detector response will suffer from broad tails, which becomes more pronounced with increasing photon energy. CZT can be formed into different shapes for different radiation-detecting applications, and a variety of electrode geometries, such as coplanar grids [Owe06] or drift strip detectors [Pam00], have been developed to provide unipolar (electron-only) operation, thereby improving energy resolution.

CZT detectors are fabricated with thin metallized electrode geometries deposited on the detector surfaces. These electrodes are then electrically biased creating an electrical field within the detector volume. When ionizing radiation interacts with the CZT crystal, electron-hole pairs are created in proportion to the energy of the incoming radiation. The negatively charged electrons and positively charged holes then migrate to the oppositely charged collecting electrodes. The resulting charge pulse is then detected by the preamplifier, which produces a voltage pulse whose height is proportional to the incident energy of the incoming photon. The signal from the preamplifier is then fed into a shaping amplifier that converts the signal into a Gaussian pulse and amplifies it. The signal can then be fed into a standard counting system or Multi Channel Analyzer (MCA) to generate the characteristic spectrum for the incoming photons.

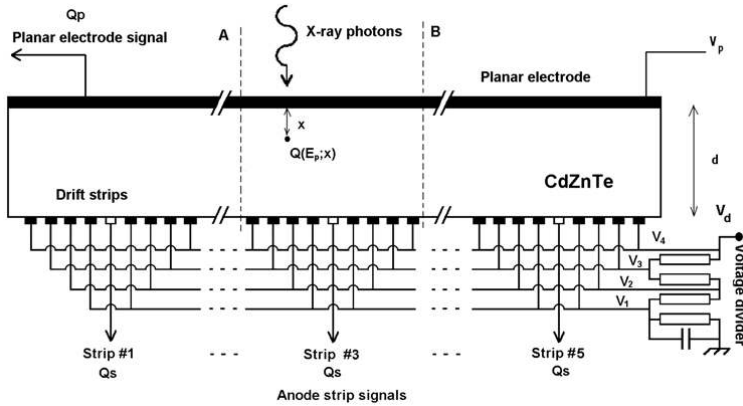


Figure 2.6: Cross section of the CZT detector with drift strips. Taken from [Kuv10].

In order to solve the problem of inefficient hole collection in the CZT detector, drift strips have been applied near the anode (see Figure 2.6). At high energies photon absorption takes place deeper below the detector surface, closer to the anode. The drift strips screens the anode from the holes, thus reducing the anode's sensitivity to the holes. The planar electrode's sensitivity to holes remains unchanged. A detailed description can be found in [Pam00, Kuv10]. Beside improvement of the spectral performance for CZT detectors, the drift strip readout technique also yields information about the interaction depth of the detected photon. The depth of interaction information (also termed depth sensing) can be derived from the ratio $R = Q_p/Q_s$, where Q_p is the planar electrode signal and Q_s the pixel signal. The quantity R is almost linearly dependent on the photon interaction depth with a value close to unity for interactions close to the planar electrode and a value close to zero for interaction near the pixel electrodes (anode). The difference in the depth profiles of interaction depth also allows for

discrimination between photons and electrons.

2.3.2 Preliminary X-ray measurements with a pixelated CZT detector

The $10 \times 10 \times 5$ mm CZT crystal is divided in a 4×4 pixels geometry for 2D imaging capability; each pixel can be read out individually. However, for this experiment the pixels have been interconnected to form 4 rows for detection (each rows consist of 4 pixels). In total three rows (one not connected) and the planar electrode were monitored for X-ray detection. The planar electrode covers the detector's surface and always produces a signal when one of the rows detects energetic radiation. It is used as a confirmation signal for energetic radiation detection. Any pulsed signal produced by one of the rows, but not seen on planar electrode, should be discarded. The common planar electrode was biased at -500 V and the pixel anodes at 0 V.

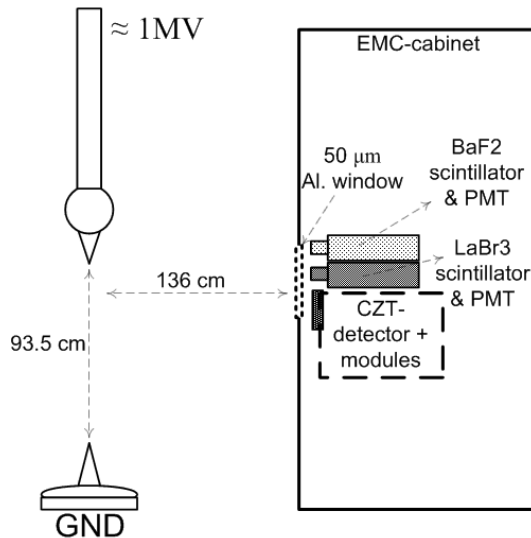


Figure 2.7: A sketch of experimental set-up, showing the three γ -detectors inside the EMC-cabinet; CZT, $\text{LaBr}_3(\text{Ce}^+)$ and BaF_2 .

The CZT detector was used in parallel with the $\text{LaBr}_3(\text{Ce}^+)$ and the BaF_2 scintillation detector. Figure 2.7 gives an impression of the experimental set-up. A burst of hard radiation produced during the surge, could be detected by all three detectors. Despite the small size of the CZT detector, a small number of detection events have been registered by the CZT detector simultaneously with the two scintillation detectors for two series of 100 positive and 100 negative discharges.

Table 2.1 summarizes the number of X-ray detections of each detector. Two of such detections are displayed below in Figure 2.8 and Figure 2.9 for negative and positive surges respectively. From the figures it is noticeable that the duration of the CZT signal is relatively slow and long compared to that of the scintillation detectors used. It is remarkable that all three detectors register energetic radiation at the same moment, considering the different types and sizes of the detectors used.

Table 2.1: X-ray detection events with CZT, $\text{LaBr}_3(\text{Ce}^+)$ and BaF_2 detectors for two series of 100 positive and 100 negative discharges.

	Positive	Negative
CZT	3	3
$\text{LaBr}_3(\text{Ce}^+)$	23	15
BaF_2	10	8

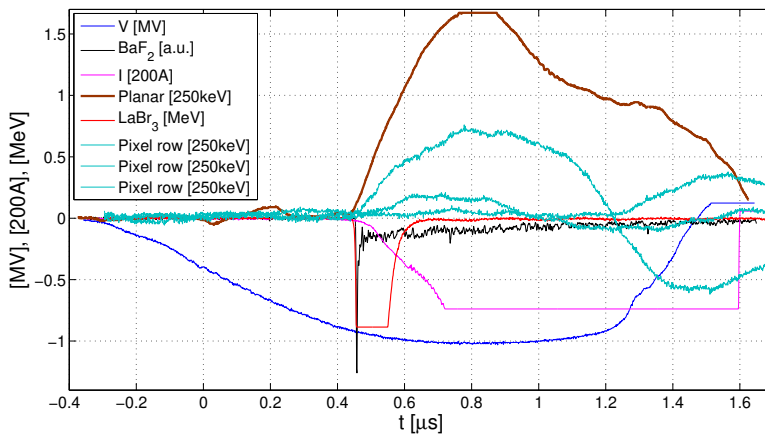


Figure 2.8: Example of a simultaneous responses of CZT, BaF_2 and $\text{LaBr}_3(\text{Ce}^+)$ detectors during a negative high voltage surge.

It is also remarkable that 4 of the events were detected with energies in the 400 keV to 600 keV band of the CZT detector. These values single are higher than those obtained with the $\text{LaBr}_3(\text{Ce}^+)$ detectors, assuming it is from single photon detection. The amplitude of the high voltage discharge was around 1 MV for positive polarity and -1 MV for negative polarity respectively. It is surprising that the pulse shapes of the CZT detected events indicate that all radiation events seems to be detected close to the detector surface (as was suggested by

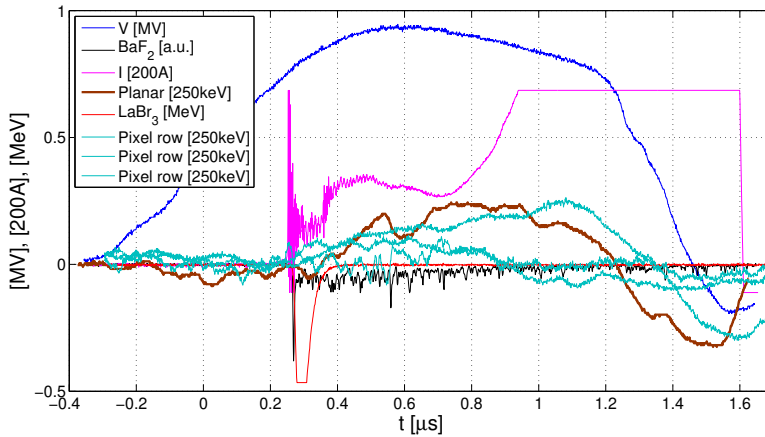


Figure 2.9: Example of a simultaneous responses of CZT, BaF_2 and $LaBr_3(Ce^+)$ detectors during a positive high voltage surge.

Carl Budtz-Jørgensen after analyzing the CZT data at his facility) and therefore most likely are electrons which have a much shorter range in CZT than photons in this energy band. On the other hand, if these events were electrons, it would have been absorbed or scattered in the 1.4 m air, the aluminium window of the EMC-cabinet and casing of the scintillation detector. It cannot be ruled out that fast electrons produce bremsstrahlung radiation locally on the detector casing, which could penetrate into the scintillator crystal. Another arguments is that it is very doubtful that in the case of positive polarity high voltage discharges energetic electrons could be emitted towards the EMC-cabinet. For negative polarity high voltage discharges this effect cannot be excluded.

This preliminary result only shows that more measurements are needed for better statistics in order to come to solid conclusions. In addition a CZT detector with a larger detector surface is also convenient for higher detection rate of energetic radiation.

2.4 Discussion and conclusions

Results from X-ray detections obtained with several scintillation detectors and a semiconductor detector have been presented in previous sections. Based on their performance and their practical use in the experimental environment, we prefer to work with the $LaBr_3(Ce^+)$ scintillation detector. The $NaI(Tl)$ scintillation detector is available in large sizes and therefore advantageous for a high radiation

detection rate. However, the decay time and the energy resolution has been exceeded by a more modern $\text{LaBr}_3(\text{Ce}^+)$ scintillation detector. From literature it is known that for energies < 100 keV the energy resolution of $\text{NaI}(\text{Tl})$ is better.

Despite the fast BaF_2 scintillation detector response, we did not manage to capture multiple X-ray photons pulses within the time window of a broadened $\text{LaBr}_3(\text{Ce}^+)$ signal. The reason for this is still unclear. According to literature the coincidence timing resolution of BaF_2 and $\text{LaBr}_3(\text{Ce}^+)$ are almost the same. With this in mind it is more favorable to use a $\text{LaBr}_3(\text{Ce}^+)$ scintillation detector, taking advantage of the good energy resolution.

Linearity of the $\text{LaBr}_3(\text{Ce}^+)$ detector during the experiments has been verified, especially for the energy range of the radiation detected. The 750 V bias applied to the PMT showed good linearity from the 59.6 keV to 1332 keV range, a deviation from linearity of 8.6% appeared at 2505 keV. For detection of higher energies the bias voltage should be reduced in order to avoid PMT saturation.

The preliminary experiment with the CZT detector has shown that the detector can be used for laboratory experiments. Proper precautions are needed in order to protect the peripheral equipment and reduce the noise level in the total system from the strong electromagnetic disturbances during the high voltage breakdown. Although energetic radiation has been recorded with this type of detector, the result was difficult to interpret and a more extensive experiment is required.

CHAPTER 3

X-RAY FROM WIRE-PLATE CORONA REACTOR

Remark: This chapter is published in Journal of Physics D: Applied Physics [Ngu10], therefore changes have been kept to a minimum with respect to the accepted paper.

This chapter presents X-ray emission detected occasionally during the streamer-corona propagation in a wire-plate corona reactor open to ambient air. A 65 kV pulse with 15 ns rise time is applied to the wire anode superimposed on a 20 kV_{dc} bias. The duration of the driving voltage pulse, approximately 110 ns, is less than 2.5 times the primary streamer transit time. Under this condition no arc discharge occurs between the wire and the cathode plates separated by 6 cm air. Measurements show that the onset of X-ray emission coincides with the initiation of the primary streamers near the wire anode. No X-rays were detected later, during or after the primary or secondary streamer development. X-ray energies ranged between 10 and 42 keV, as detected by a LaBr₃(Ce⁺) scintillator photomultiplier combination. Time resolved imaging of the streamer propagation highlights the different stages in the streamer discharge process. The energetic electrons originate near the anode, at the moment of streamer initialization.

3.1 Introduction

Repetitive streamer-corona plasma created by pulsed high voltage nanosecond discharges has widely been used in industrial applications, in particular in chemical processing [Yan98, Win06a, Vel00, Bec05, Win06b]. A strong overvoltage is needed to create such streamer-corona plasma. In the pulsed corona setup described in [Win07] positive voltage pulses of the order of 110 ns are applied,

with and without dc bias. The good reproducibility of the discharges allows a detailed study into the physics of the gas discharge. Here we report that X-rays may occur at the early stage of the discharge. Experimental studies involving X-ray radiation in short atmospheric gas discharges have been presented in [Sta67, Kos06, Rep08, Bab09]. Still, the occurrence of electrons with energies of up to the full applied voltage is not fully understood. This motivated our experimental study of X-ray generation in transient streamer like discharges. Nanosecond fast photography provided detailed characterization of the discharge phenomena and the streamer formation, in relation to the voltage pulse and the X-ray generation. The work parallels investigations on the development of metre-long discharges (Chapter 4) in a spark gap connected to a lightning surge generator where the discharge and full breakdown following the streamer-leader phase are difficult to avoid.

3.2 Experimental set-up and procedure

The corona reactor consists of two grounded plates and a single wire in between (Figure 3.1). The plate height and width are 1.10 m and 0.25 m, respectively; the distance is 0.12 m. The 0.40 mm diameter stainless steel wire of 0.90 m length runs over the centre line between the plates.

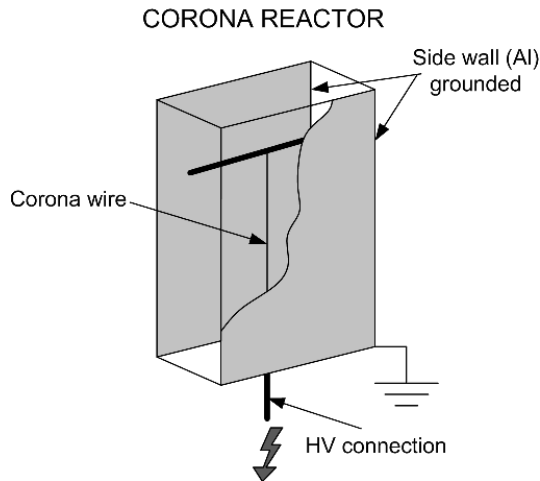


Figure 3.1: Wire-plate corona reactor.

A polycarbonate cover allows controlled airflow in the reactor. The power source is based on a resonant pulse forming line. A two-stage transmission line transformer doubles the voltage; the transmission line length determines the pulse duration

of 110 ns. The positive high voltage pulse has a rise/fall time of 15/25 ns at the wire. The pulse repetition rate is 10 Hz. In the measurements a dc bias of +20 kV has been applied. Because of the short pulse duration with regard to the primary streamer transit time, no total gap breakdown occurred. Still, the matching of the source to the corona reactor is difficult to control because of the varying reactor load impedance (discussed in [Win07, Ch.4]). Minor reflections indeed occurred in the voltage waveform.

A differentiating-integrating measuring system with 80 MHz bandwidth [Deu06] captures the voltage and current waveforms. The major advantage of this system is the large immunity to the interference generated by the discharge. The dc bias is measured separately. The current and voltage data are directly stored on a fast oscilloscope with 3 GHz analogue bandwidth and 10 GSamples \cdot s $^{-1}$.

Figure 3.2 shows the floor plan of the measurement setup. X-rays are detected by a LaBr₃(Ce⁺) scintillator with associated photomultiplier placed inside an EMC-cabinet. The detector was calibrated using a ¹³⁷Cs source with γ -energy of 662 keV. The linearity was checked by the 59 keV radiation from a ²⁴¹Am source and the 1.17 and 1.33 MeV radiation of ⁶⁰Co. A model response curve was obtained by averaging a large number of γ -signals in the ¹³⁷Cs photopeak. We used this model pulse to fit the X-ray data and determine the energy absorbed in the scintillator. The detector faced the open side of the corona reactor, and was aimed at the wire (anode) between the grounded plates (cathode). The aluminium casing of the scintillation crystal in combination with the aluminium window on the EMC-cabinet has a 1/e cutoff energy in the order of 17 keV. In addition, the 0.6 m distance in air between anode and detector provided additional absorption of 30% at 10 keV and of 1/e below 5 keV. The solid angle Ω of the detector was 3.2×10^{-3} sterad as viewed from the nearest point on the wire anode.

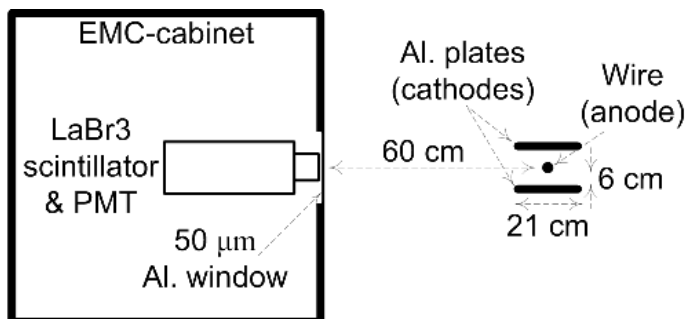


Figure 3.2: Floor plan of measurement setup, showing the γ -detector inside an EMC-cabinet. A thin aluminium window provided effective shielding against electromagnetic interference but allowed hard X-rays to pass.

3.3 The streamer phase

The initial phase of the corona is the domain of streamers, characterized by a large electric field enhancement at the streamer head. The strong local electric field ensures a positive net ionization coefficient, aided by photoionization. Many new free electrons are created directly in front of the streamer head. The streamer propagates mainly in the direction of the field enhancement, resulting in the channel-like appearance of the streamer, see Figure 3.3.

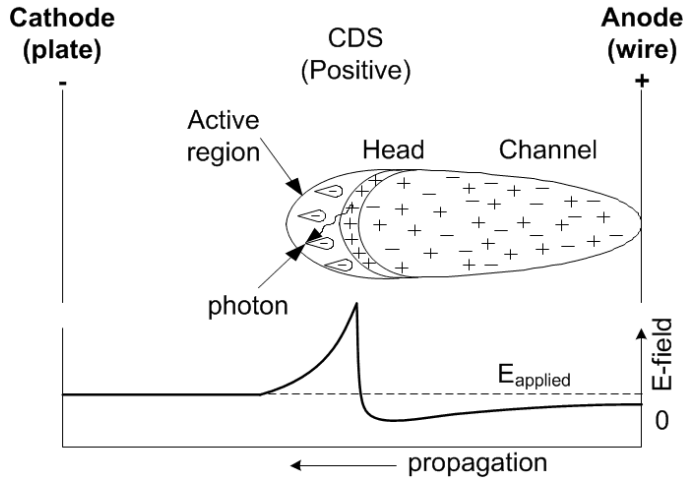


Figure 3.3: Schematic view of a cathode directed streamer.

Experimental verification of this model is presented in Figure 3.4. This picture has been published earlier in [Win08] and is used here again to demonstrate the correlation between X-ray production and the different phases in the streamer development. The series of photographs, taken with a fast intensified charge-coupled device (ICCD) camera, shows the development of the streamers starting at the wire and directed to the reactor wall. With the positive polarity, streamers appear simultaneously all over the wire. Figure 3.4(i) shows the times at which the photos were taken relative to the voltage pulse. The discharges are repetitive and the current and voltage waveform measured were consistent for individual discharges. In this manner it is possible to link the pictures taken earlier with the X-ray detection performed later. Soon after the voltage rise primary streamers form and propagate across the gap (Figures 3.4(a)(f)). At the moment the primary streamers reach the wall or cathode (Figure 3.4(f)), secondary streamers start at the wire [Mar81, Sig84, Tar02]. The secondary streamers travel only partly into the inter-electrode gap (Figures 3.4(f)(h)) depending on

the duration of the applied voltage. These streamers remain attached to the anode. More information on the streamer history in this setup can be found in [Win08]. Theoretical studies that adapt conditions comparable to those in the experiments show that the typical maximum electric fields in the streamer head are $100\text{-}200\text{ kV}\cdot\text{cm}^{-1}$ [Bab97, Mor97, Kul98, Nai09].

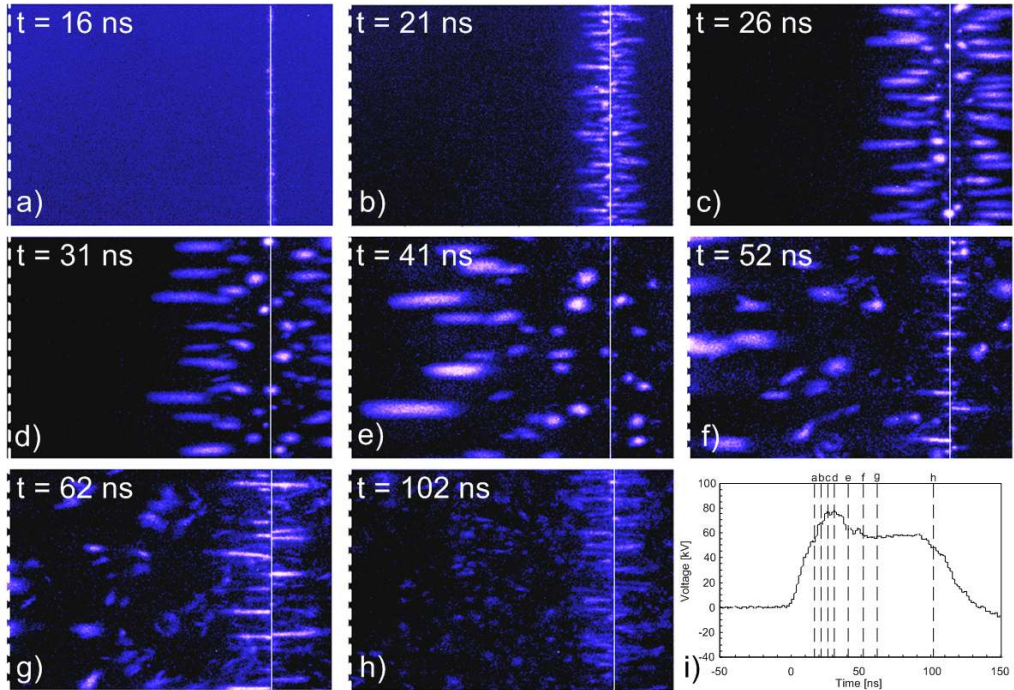


Figure 3.4: Time resolved side view ICCD pictures for the voltage waveform shown in (i). Pulse parameters: pulse width 110 ns, pulse voltage 74 kV with a rate of $2.7\text{ kV}\cdot\text{ns}^{-1}$. Picture size is $7 \times 5\text{ cm}^2$. White line: reactor wire (anode). Dotted line at the left: reactor wall (cathode). The times at which the pictures were taken, relative to the start of the voltage pulse, are shown in the top left corner of each picture and is also indicated in graph (i) [Win08].

3.4 X-ray detection

A typical example of an X-ray signal is given in Figure 3.5. Some noise couples into the signal recording channel. The raw X-ray data (thin line) are filtered by applying a moving average over 75 points (equivalent to 7.5 ns). All X-ray pulses presented onwards have been smoothed similarly. At time $t = 0\text{ ns}$ the

X-ray photon is absorbed by the scintillator. This time was determined by the comparison of the signals from a 4 ns fast BaF_2 detector and the $\text{LaBr}_3(\text{Ce}^+)$ detector, looking simultaneously to a nanosecond X-ray burst from the lightning surge generator (see Figure 4.5). Corrections were applied for delays in the PMT, the cables and the recording instruments. The travel times of X-ray over the 60 cm distance, which is about 2 ns, can be neglected. The accuracy of $t = 0$ ns determination is 3 ns or better.

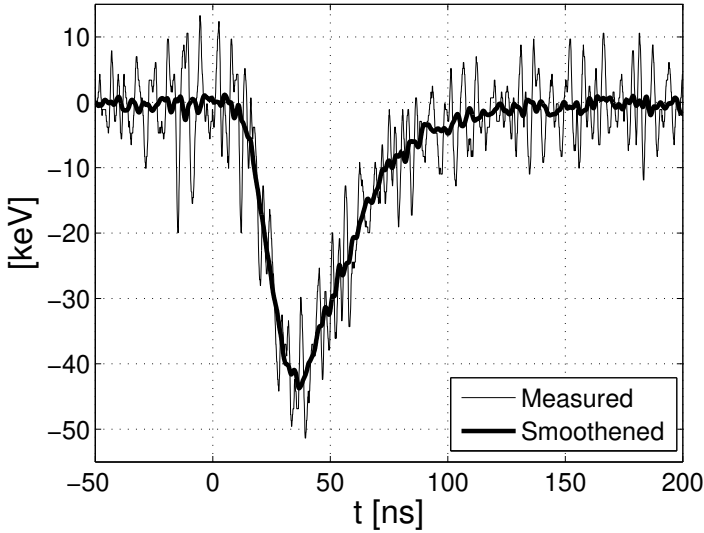


Figure 3.5: Example of X-ray signal measured from the corona reactor with a $\text{LaBr}_3(\text{Ce}^+)$ γ -detector.

Figure 3.6 (top) shows the voltage applied to the reactor and the current entering the reactor. The current comprises both the capacitive current to establish the electric field and the corona current due to the moving charges. As in [Rep08], we tentatively determine the onset of the corona current t_s by extrapolation of the linear current rise between $t = 20$ and 45 ns to zero current (dotted line). The dip in voltage and current at 92 ns is caused by reflection due to load mismatching of the corona reactor and power source.

In 17 out of a series of 5795 streamer-corona discharges X-rays were observed. All signals could be fitted to a single model pulse within the noise. This indicates that each of these X-ray pulses was a single photon event or a simultaneous detection of several photons. The X-ray energies were always below electron charge q times the total voltage, in agreement with an assumed Bremsstrahlung process and single photon detection. The number of X-ray quanta per streamer

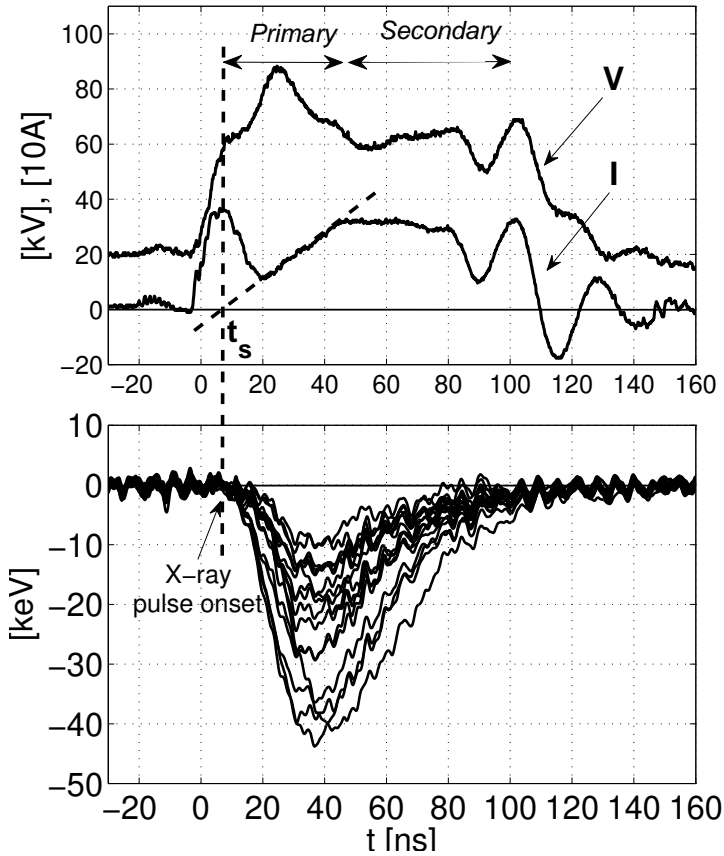


Figure 3.6: *Top: curve V: A single voltage pulse is shown, representative for all discharges. A dc bias of 20 kV was applied. I: the current measured at the reactor input. Bottom: 17 X-ray pulses detected in a series of 5795 discharges. All X-quanta occurred at the start of the primary streamer, at $t_s = 8$ ns (arrow).*

X_s can be estimated from the measured occurrence $N = 17/5795$ and from the number of streamers per metre wire $n \approx 1400$ obtained from the photographs [Win08]:

$$N = nX_s \int_{-l_w/2}^{l_w/2} \Omega(l) e^{-\mu\rho\sqrt{l^2+d^2}} dl,$$

where l_w is the length of the wire (0.9 m), μ is the absorption coefficient of air taken from the NIST tables [NIS], ρ is the density of air and $\Omega(l) = \pi r^2 / (l^2 + d^2)$ is the solid angle of the detector seen on the wire at position l at the

distance $d = 60$ cm. The detector is nearly spherical with a radius of 19 mm. The absorption of the X-ray quanta in air and aluminium windows does not influence the X-ray detection substantially. The resulting X_s is about 2×10^{-3} . This is far below what we observed in the setup with the lightning surge generator, where we recorded X-rays in all 1 MV discharges; the energies were hundreds of kiloelectronvolts. It cannot be attributed to a diminishing detection efficiency of the $\text{LaBr}_3(\text{Ce}^+)$ detector [Ilt06]. To understand the difference, one may assume that the underlying assumption of isotropic X-ray emission is incorrect. But then it should be sharply peaked, for instance in the streamer propagation direction. Or one has to accept the low production as a fact. For the records of Figure 3.6 the energy absorbed in the scintillator is a good representation of the X-ray quantum energy, since partial escape after a Compton scattering is less likely. This was confirmed for 59 keV ^{241}Am quanta.

However, the time of the onset of the X-ray signals is more important here; it coincides within the experimental accuracy with t_s , the initialization of the primary streamers, when the wire starts to glow. Figure 3.4(a) gives an impression of this moment. All X-ray waveforms detected initiated at the same time t_s of 8 ns. This is also the moment when the electric field near the wire is high enough for the formation of primary streamers. Simultaneously a large fraction of the total voltage drop is concentrated in the first millimetres near the wire. A short distance facilitates the electrons to acquire the large energy necessary for X-ray formation. A two-dimensional calculation shows that 50% of the voltage drop occurs over the distance of 10 times the wire diameter or 4 mm neglecting effective enlargement of the wire by corona. No X-rays were measured after the initiation of the primary streamers or during the development of the secondary streamers. This proves that the X-rays were produced near or at the anode only. This observation is in agreement with the experimental results from Stankevich and Kalinin [Sta67], where they concluded (without any data on the voltage or current waveforms) that electrons in the initial stage of a spark discharge can gain an amount of energy comparable in magnitude to the applied voltage.

We repeated the measurements with several larger series of discharges; all showed the same picture as presented in Figures 3.4 and 3.6. Although the X-ray detection rate was low, in 0.75% of the discharges, the recurrence in timing of detection excludes background radiation or other sources to trigger the γ -detector other than the high energetic photons coming from the corona reactor.

The X-ray recordings presented in Figure 3.6 show similarities with [Rep08]. The polarity and the type of discharge are different, but the timing and conditions of X-ray emission are comparable.

3.5 Discussion

If we consider the data on dynamic friction force of electrons in air at ground pressure as a function of electron energy presented by *Moss et al* in [Mos06], it seems that some electrons have managed to pass the absorption peak around the 100 eV. This would imply that the local electric field near the streamer head could surpass E_c ($260 \text{ kV}\cdot\text{cm}^{-1}$), the thermal runaway threshold [Gur61], considering that the energies detected are in the order of 10 to 42 keV. From the plot in Figure 3.6 one can conclude that this high electric field is only present at the moment of streamer initialization where the onset of X-ray takes place.

Recent observations of X-ray and gamma ray bursts in the earth's atmosphere have been linked to lightning. Existence of high energetic electrons during thunderstorm activity has been confirmed [Moo01, Dwy05a], but the mechanism producing these energies is still under debate [Neu08]. The results presented here show that streamer discharges are also a realistic alternative source of high energy electrons as suggested by *Moss et al* in [Mos06], providing seed electrons to the relativistic runaway electron avalanche model proposed by *Gurevich et al* [Gur92].

Measurements of the local electric field have been performed in low pressure xenon with paraboloid electrodes [Wag07]. Especially for atmospheric discharges with highly inhomogeneous fields as studied here, it is difficult to create a stable or periodically reproducible streamer-corona plasma. This makes it hard to determine the local electric field experimentally. X-ray measurements like these presented here contribute to a better understanding of the electric field distribution in a streamer development, as these serve as a test for models.

3.6 Conclusion

This experimental study concerned the pre-breakdown phase in a wire-plate corona reactor. Occasional X-ray detection occurred simultaneously with the onset of the primary streamer. The electric field near the anode wire or streamer head is strong enough to allow few electrons liberated by photo or field ionization to overcome the dynamic friction force due to collisions with air molecules and to gain sufficient energy to produce the X-rays. The streamer-corona plasma can thus be considered as a new configuration to study runaway electrons.

CHAPTER 4

MULTIPLE X-RAY BURSTS FROM LONG DISCHARGES IN AIR

Remark: This chapter is published in Journal of Physics D: Applied Physics [Ngu08], therefore changes have been kept to a minimum with respect to the accepted paper. Comments on the paper are added at the end of this chapter.

In this chapter experimental investigation on X-ray bursts emission from metre-long discharges in air is treated. A lightning surge generator generates a high voltage surge with a $1.2 \mu\text{s}$ rise time. The generator fed a spark gap of two pointed electrodes at 0.7 to 1.2 m distances. Gap breakdown occurred between 0.1 and $3 \mu\text{s}$ after the maximum generator voltage of approximately 850 kV. Various scintillator detectors with different response times recorded bursts of hard radiation in nearly all surges. The bursts were detected over the time span between approximately half of the maximum surge voltage and full gap breakdown. The consistent timing of the bursts with the high voltage surge excluded background radiation as the source for the high intensity pulses. In spite of the symmetry of the gap, negative surges produced more intense radiation than positive. This has been attributed to additional positive discharges from the measurement cabinet which occurred for negative surges. Some hard radiation signals were equivalent to several MeV. Pile-up of lesser energy X-ray quanta occurs, but still with a large fraction of these with an energy of the order of 100 keV. The bursts occurred within the 4 ns time resolution of the fastest detector.

4.1 Introduction

As early as 1924 Wilson [Wil24] stated that: "by its accelerating action on particles the electric field of a thundercloud may produce extremely penetrating

corpuscular radiation”. High energy radiation has indeed been associated with lightning, as it has been observed in measurements from space [Fis94, Smi05], in balloon flights [Eac96] and at surface level [Moo01, Dwy05a] (see section 1.2.3).

We studied sparks of the order of 1 m length in the laboratory, and focussed our attention to where and when in the developing discharge channel the high energy radiation is generated. In comparison with earlier work [Dwy05b] we added a larger number of measurements to allow a statistical analysis. The setup will be presented in detail, because it strongly influenced the timing, intensity and position of the hard X-ray generation, as discussed in section 4.3. A more recent paper [Rah08] presents results on a careful experiment, similar to but independent of ours; we discuss similarities and differences in section 4.4.

The scintillator detector used in most of our measurements has a good energy resolution for single γ -ray quanta in the photopeak. However, the relation between detector output and X-ray or γ -quantum energy is generally not straightforward, as will be discussed in section 4.2.1. We tried to resolve the ambiguity by placing lead or aluminium absorbers of various thicknesses in front of the detector. Ultimately, a theoretical description of the developing discharge should provide an energy distribution of electrons. The Bremsstrahlung process further complicates the relation between electron and radiation energy.

4.2 Experimental set-up and procedure

For our experiments we used the 2 MV twelve stage Marx generator [Kuf00] (p.61) in the high voltage laboratory at Eindhoven University of Technology. The voltage waveform of the unloaded generator is a standardized lightning surge with 1.2 μ s rise time and 50 μ s decay to half-maximum. The surge amplitude and polarity can be chosen. The 9 m tall 1:2000 high voltage (HV-) divider is a part of the waveshaping circuit.

Figure 4.1 shows the floor plan of the setup. A spark gap consisting of two pointed aluminium electrodes (cone angle 21° , tip radius about 1 mm) was placed on insulating stands at 2 m above the floor. One electrode was connected to the divider high voltage end, the other to the conducting floor. The 0.7 m distance between the tips typically used ensured full gap breakdown at approximately 1 MV surge voltage within one or a few microseconds after the maximum voltage V_{max} . Of course this delay depended on the electrode distance and the Marx generator setting.

A grounded EMC-cabinet [Hou97] faced the spark at the distance of $d = 0.8$ m and more. The closed EMC cabinet contained the γ -detector and all recording equipment. A 0.05 mm thick, 15 cm diameter aluminium window allowed the

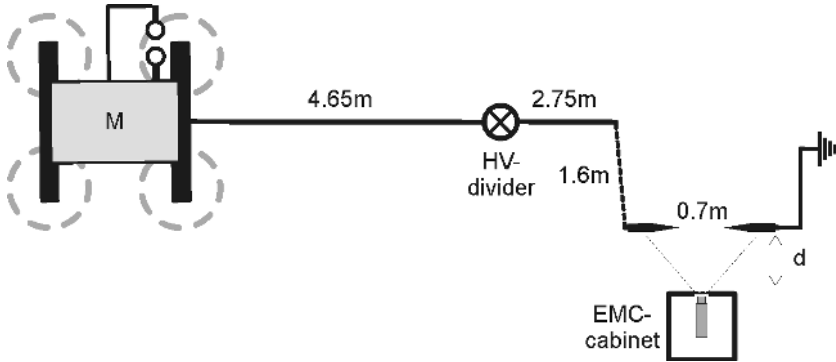


Figure 4.1: Floor plan of the setup, showing the position of Marx generator (M), HV-divider, 0.7 m spark gap and EMC cabinet with detector at the distance d from the gap.

hard radiation quanta to pass. It also maintained sufficient shielding against the surge electromagnetic interference. This was demonstrated first by a small number of high voltage surges, when no hard radiation was detected and only the noise level of the oscilloscope was recorded. Second, we used three scintillation detectors with response times between 230 and 4 ns, and all the detectors produced signals in the high voltage surge measurements with waveforms similar to those obtained for individual gamma quanta from e.g. a ^{137}Cs γ -source, outside the high voltage laboratory. Our change of scintillation detectors is equivalent to the comparison of detector output with and without scintillator as applied in [Dwy05a, Dwy05b]. Third, insufficient cabinet shielding or power supply surges usually lead to an oscillating waveform. This has never been observed with the oscilloscope sensitivity used in our measurements.

The 8.5 m distance between the Marx generator and the spark gap reduced the chance that the detector captured hard radiation from the twelve generator spark switches.

A Tektronix TDS 3054 four-channel 8 bit digital oscilloscope recorded the HV-divider output after further reduction by a factor of 40. The scope also registered the current through the grounded electrode via a Pearson 110 current probe with a rise time of 20 ns. The probe was mounted near the floor, at the grounded end of a 2 m long wire to the electrode. The γ -detector output was most often fed into two channels with a factor of 10 different in sensitivities in order to enhance the dynamic range. After a high voltage surge all data were automatically saved on a computer. This allowed uninterrupted measurements, and many hundred surges have been recorded.

4.2.1 γ -detectors

We used three types of γ -detector with NaI(Tl), BaF₂ and LaBr₃(Ce⁺) scintillator crystals. All scintillators were attached to photomultipliers with adequate speed. These detectors' characteristics have been detailed in Chapter 2. In Figure 4.2 we compare the first two materials. The γ -source was a sample of ¹³⁷Cs emitting characteristic γ s of 662 keV. A total number of 5000 pulses have been recorded without further signal processing by an oscilloscope with 8 bit amplitude resolution. The pulse peak values were determined, and we plotted in Figure 4.2 the number of occurrences in bins of 1 resp. 2 mV versus the peak values. The spectra show that a direct interpretation of photomultiplier output pulse height in terms of incoming γ -quantum energy is not allowed. A γ -quantum can be absorbed completely in the scintillator and is then detected in the photopeak P. However, it is more likely that the γ -quantum undergoes Compton scattering. When the scattered γ -quantum escapes the scintillator the output signal will be correspondingly smaller as shown by the large and broad Compton ridge C.

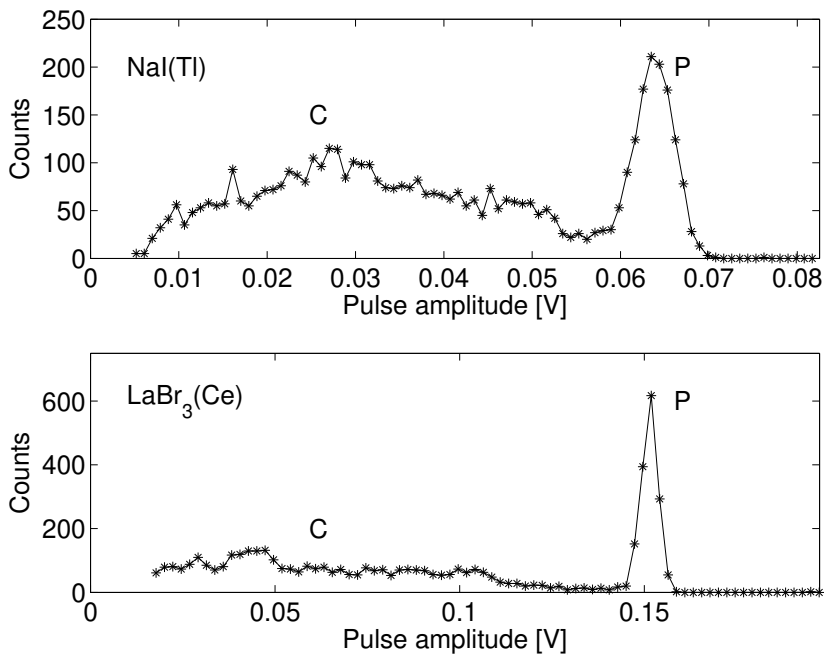


Figure 4.2: ¹³⁷Cs pulse height spectrum for NaI(Tl) and LaBr₃(Ce⁺) detectors of 5000 pulses recorded by an 8 bit resolution oscilloscope. The horizontal axes have been scaled to coincide on the photopeak

Several characteristics of three materials are summarized in Table 4.1: (a) the

Table 4.1: *Characteristics of the three scintillator materials in a Philips PW4119 detector, a Brilliance 380 detector by St. Gobain [StG] and a BaF₂ detector by Scionix.*

	NaI(Tl)	BaF ₂	LaBr ₃ (Ce ⁺)
(a) # Photons/keV	38	1.8	63
(b) Rise/fall (ns)	40/230	--	11/23
(c) FWHM (ns)	270	4	38
(d) En. resolution	7.8%	12%	3.3%
(e) Compton/Photo	7	--	4
Provider	Philips	Scionix	St. Gobain

number of optical photons per kiloelectronvolts absorbed γ -energy, (b) the rise and fall times of the output pulse, (c) the full width in time at half height of the light output. The width at half height of the photopeak in an amplitude spectrum for ¹³⁷Cs γ s is given in row (d), now recorded [StG] with adequate waveshaping electronics and a multichannel analyser. Row (e) shows the probability ratio of detection in the Compton ridge or in the photo peak.

Introductory measurements were performed with the NaI(Tl) detector. It was quickly superseded by the modern LaBr₃(Ce⁺) detector because of its faster response and better energy resolution. The 0.5 mm thick aluminium front of the scintillator encasement reduces the detection efficiency below 17 keV. For the measurements discussed here the time resolution of the LaBr₃(Ce⁺) detector is about 4 ns on the 11 ns leading edge. A few measurements have been taken with a BaF₂ detector. The signal of this detector is composed of a fast component of 4 ns (FWHM) duration and a slow component. We only regarded the fast component.

Because most of the data to be presented have been obtained with the LaBr₃(Ce⁺) detector, we determined its response in more detail. A model pulse waveform was obtained from ¹³⁷Cs 662 keV radiation. In order to reduce digitizing noise, we averaged the records of 1200 pulses with amplitudes inside a window of 10% around the photopeak. This averaged waveform was then available as a numerical time series. It included the response of the photomultiplier, and deviated substantially from the bi-exponential waveform which suited well for NaI(Tl); see also section 4.3.1. With this model waveform we determined the equivalent energy of the X-ray pulses from a high voltage surge, by adjusting time and amplitude in a least square fit procedure. This implicitly assumes that the response does not depend on energy or signal amplitude. The fit was even successful when the signal was slightly clipped by the oscilloscope, leaving the clipped data out of the fit. The procedure has been verified by using data

recorded simultaneously on two channels with different sensitivity, with one dataset clipped. For appreciably broadened X-ray pulses we fitted the data to a train of model pulses with the smallest number of pulses possible. An example of such a train fit is presented in section 4.3.3. Hereafter all amplitudes are expressed in equivalent radiation energy using the ^{137}Cs calibration. But again, we caution for a direct interpretation of signal amplitude into equivalent energy neglecting Compton scattering. On the other hand, it may also occur that several quanta are absorbed within the response time of scintillator and photomultiplier. Pile-up of their signals then occurs.

A remark about wording: γ -rays are commonly associated with nuclear processes, X-rays involve electrons. Hard X-rays and soft gammas overlap in energy. We retained the term γ -detector because of the usually intended application.

4.3 Experimental data

4.3.1 Comparison of γ -detectors

We first present two measurements to compare the detectors most used. The NaI(Tl) detector recorded signals in 50% of the positive high voltage surges, but much less for negative polarity. Figure 4.3(a) shows an example of a measurement: the high voltage surge V_{HV} measured by the HV-divider together with the simultaneous record by the NaI(Tl) detector. The X-ray signal is displayed inverted for convenience. The gap electrode distance was 1.20 m. This record is similar to those published in [Dwy05b]. Our high voltage surge started at time $t = 0.75 \mu\text{s}$, reached the maximum at $t = 2.50 \mu\text{s}$ and collapsed due to the spark gap breakdown at $t = 3.85 \mu\text{s}$, and then developed in a damped oscillation. The response of the γ -detector showed two barely resolved peaks at $t = 2.18$ and $2.30 \mu\text{s}$. The response could be fitted to within the noise by two bi-exponential model pulses with rise and fall time constants shown in 4.1. The vertical bars in Figure 4.3 indicate the value and time of the maximum of the model pulses. Fitted equivalent amplitudes corresponded to energies of 0.27 and 0.17 MeV respectively. One observes that the second pulse starts in the decay time of the first.

Figure 4.3(b) shows an early measurement with the $\text{LaBr}_3(\text{Ce}^+)$ detector. The electrode distance was 0.7 m, which led to a shorter time to breakdown than in Figure 4.3(a). The solid angle Ω of the detector is about 1.4×10^{-3} sterad as viewed from the electrodes or developing spark. Five X-ray pulses can be recognized with equivalent energies of 0.05, 0.13, 0.28, 0.14 and 0.16 MeV in order of occurrence.

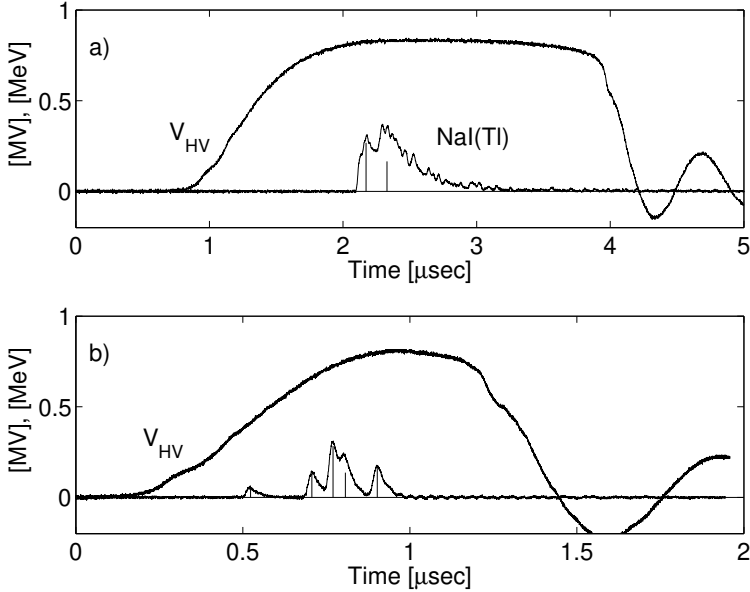


Figure 4.3: (a) Positive high voltage surge V_{HV} with 830 kV maximum and the signal from the NaI(Tl) detector shown inverted, with bars indicating the fit amplitude and time. (b) An 830 kV positive surge (V_{HV}), with the signal from the LaBr₃(Ce⁺) detector inverted. Five pulses are distinguished, with equivalent energy up to 0.28 MeV. Please note the difference in time scale with respect to panel (a). The longer pulse duration in panel (a) stems from the larger gap distance: 1.2 m for (a) and 0.7 m for (b).

For the measurement with the NaI(Tl) detector, the electrodes were covered by a thin lead foil. For the LaBr₃(Ce⁺) detector, the electrodes were aluminium. No difference between the radiation production was observed, as will be discussed in section 4.4.

4.3.2 Positive high voltage surges

We made two runs of 25 high voltage surges with 0.8 to 1.0 MV positive on the floating electrode. In all 50 surges, hard radiation has been observed with the LaBr₃(Ce⁺) detector. Four X-ray pulses with equivalent energies up to about 700 keV can be recognized in the example shown in Figure 4.4. The amplitude and time of the X-ray pulses again resulted from the fit to the model pulse. The top part includes the current I_g through the grounded electrode. The leader current started at $t = 0.8 \mu\text{s}$ and the gap broke down completely at $t = 1.5 \mu\text{s}$. This time interval coincided with the detection of the X-rays. With this current

range, the capacitive current that charges the spark gap electrodes (before $t = 0.8 \mu\text{s}$ or before leader formation) is too small to be resolved.

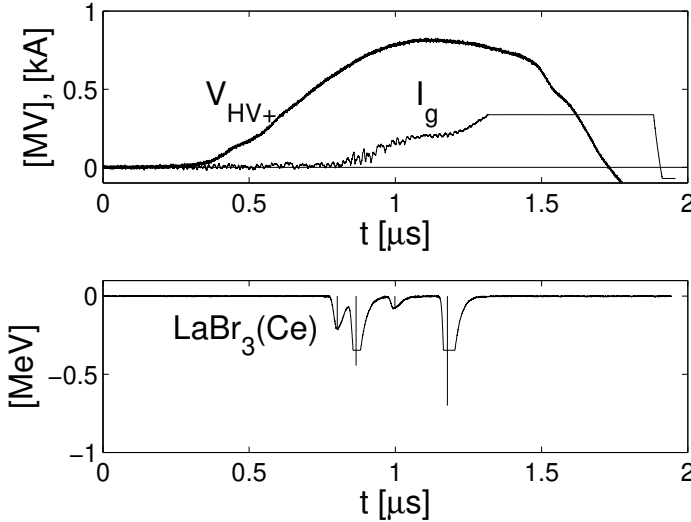


Figure 4.4: Positive surge V_{HV} with 810 kV maximum, shown with the current I_g during the leader initiation phase. At $t = 1.5 \mu\text{s}$ the gap breaks down. Four X-ray pulses can be distinguished. The γ -detector and current signals are clipped by the oscilloscope. The vertical bars indicate the maximum equivalent energy and its timing obtained by the fit.

The majority of X-rays occurred after about 75% of V_{max} . In contrast to [Dwy05b], none occurred at the start of the surge or at gap breakdown. The timing links the X-ray production to the streamer/leader formation. For most positive surges the equivalent energy per X-ray pulse was smaller than $q \cdot V_{max}$. These pulses could be fitted to the model pulse down to the noise level. This indicates that these pulses corresponded either to a single X-ray quantum or to the simultaneous detection of several lesser energy quanta well within the 4 ns detector time resolution of $\text{LaBr}_3(\text{Ce}^+)$. One of the surges produced an X-ray pulse with equivalent energy of 3 MeV; it appeared slightly broadened in time. Since it is hard to imagine that a single 3 MeV quantum is produced in our 1 MV discharges, we favour the interpretation in terms of a pile-up of several quanta within the detector time resolution. In line with this interpretation, we will use the term ‘burst’ rather than ‘pulse’ hereafter.

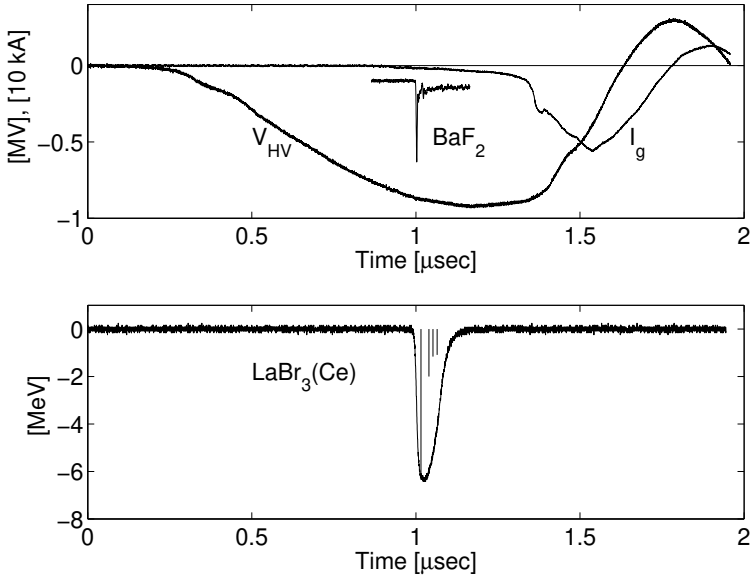


Figure 4.5: A negative 875 kV surge, shown with the current I_g and X-ray signal (arbitrary units) from an uncalibrated BaF_2 detector alongside the $\text{LaBr}_3(\text{Ce}^+)$ detector. The lower part of the figure shows the signal of the $\text{LaBr}_3(\text{Ce}^+)$ detector and the fitted amplitudes of a train of four pulses.

4.3.3 Negative high voltage surges

With the same setup negative high voltage surges always produced much stronger X-ray signals, with peak equivalent energy per burst of several MeV, a few even up to 30 MeV as determined from the maximum detector output. Figure 4.5 shows an example with peak value equivalent to 6 MeV. The distance between cabinet and arc was 0.9 m. With 76 ns FWHM the $\text{LaBr}_3(\text{Ce}^+)$ signal is significantly broadened compared with the model waveform (38 ns, see 4.1). Also the peak is flattened appreciably. In a series of 20 surges 14 showed a $\text{LaBr}_3(\text{Ce}^+)$ signal with averaged peak value of 5.8 ± 1.3 MeV, all significantly broadened in time. The broadening may be attributed to (a) afterglow in the scintillator, (b) saturation of the photomultiplier or (c) distribution in time of the X-rays. Cause (a) is unlikely because of the decay time data presented in [Loe02]; so there remains a combination of (b) and (c). We reduced the voltage of the photomultiplier and thereby its gain. The broadening remained. We fitted a time series of model pulses to the measured X-ray signal. The result is included in Figure 4.5 by the vertical bars indicating values and times of the maxima of the individual model pulses. In an attempt to resolve these strong signals further in time, we had

installed a fast BaF₂ detector directly next to the LaBr₃(Ce⁺). This detector was only available for a short period and was not calibrated. The top part of Figure 4.5 also shows the record for the BaF₂ detector as inset on the same time scale. The single fast response of BaF₂ on the burst coincided with the onset of the LaBr₃(Ce⁺) signal. This was also observed in 12 out of the 14 surges mentioned before. Consequently we favour the interpretation that the large LaBr₃(Ce⁺) signal is stretched in time due to saturation of the photomultiplier. The sum of the amplitudes obtained from the fit is a lower limit for the scintillation light seen by the photomultiplier.

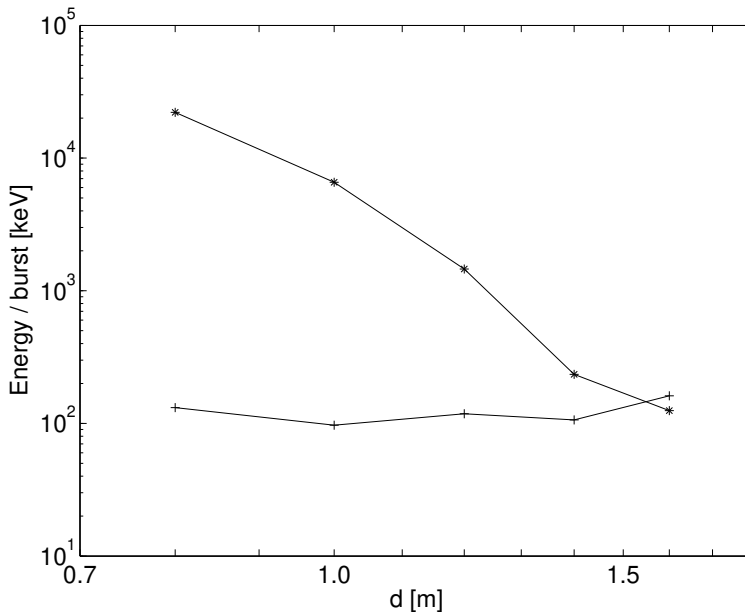


Figure 4.6: Energy per burst for positive (+) and negative (*) discharges, as a function of distance d between cabinet and spark gap.

4.3.4 Distance variation

The large differences between X-ray production of the positive and negative surges was not compatible with the symmetry of the spark gap. In order to gain insight in where the X-rays were produced, the gap was placed at different distances from the EMC cabinet (d in Figure 4.1) and a few tens of surges were produced at each position. The fit procedure gave the total equivalent energy per burst as sum of the fitted amplitudes. Surges where multiple bursts could be recognized were also analyzed this way. Figure 4.6 shows the result. In the case

of negative surges the energy per burst decreased rapidly for larger distances, approximately proportional to d^{-7} , and approached the value for positive surges at $d = 1.5$ m. For positive surges the variation was much less, if any at all. For a point-like source a d^{-2} behaviour would be expected neglecting air absorption. A line-like source would rather show to be proportional to d^{-1} .

Careful inspection by unaided eye revealed that for small d arc initiation took place on the EMC cabinet with negative surge polarity, often on a ring holding the aluminium window. Most likely, X-rays were produced also there, right in front of the detector. No such phenomena were observed for larger distances d or positive surges. This is in agreement with the X-ray abundance in negative surges at small d . Full breakdown to the cabinet occurred seldom at any d .

4.3.5 Absorber

A few measurements on negative surges have been taken with two $\text{LaBr}_3(\text{Ce}^+)$ detectors, placed alongside in the EMC cabinet. One detector was fully wrapped in a 1.5 mm thick lead foil. This foil provides a $1/e$ cutoff at 1.4 MeV, derived by the mass absorption coefficient from the NIST database [NIS]. It should be noted that these coefficients include all scattering mechanisms and assume single energy quanta and a monochromatic detector. Our detectors are not tuned for a single energy and will also record lower energy quanta emerging from the absorber after Compton scattering.

Figure 4.7 shows the results for a 0.88 MV surge. The distance d was 0.9 m. The peak value of the largest X-ray burst at $t = 1 \mu\text{s}$ was equivalent to 19 MeV for the γ -detector without absorber; again the signal was widened in time to a FWHM of 79 ns. The total equivalent energy obtained from a fit was 43 MeV. For the one wrapped in lead the largest burst corresponded to 3.5 MeV; it was not appreciably widened. The total energy was 4.7 MeV. The strong reduction of the signal by the lead agrees with the fact that the larger signal consists of a pile-up of many lesser energy X-ray quanta. If one assumes that quanta are evenly distributed in space and energy over both detectors, and one assumes that only the high energies contribute to the burst signals, the observed ratio of the signals $43/4.7 = \exp(2.2)$ can be converted into a mass absorption coefficient μ of $1.3 \text{ cm}^2 \cdot \text{g}^{-1}$. With the NIST XCOM tables [NIS], the value of μ corresponds to quantum energies between 90 and 150 keV. For the smaller burst at $t = 0.9 \mu\text{s}$ a similar analysis leads to $\mu = 2.2 \text{ cm}^2 \cdot \text{g}^{-1}$ and an energy of about 80 keV. The energies are not very sensitive to variations of μ .

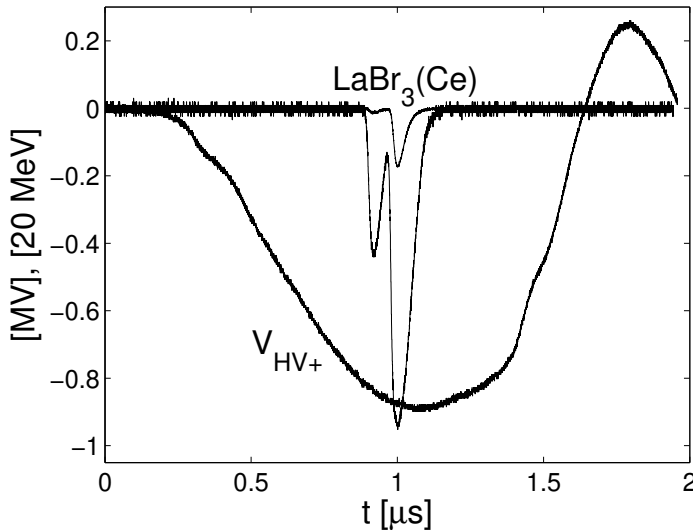


Figure 4.7: Negative surge and X-ray signals seen by two detectors, one without (large signal) and one with a 1.5 mm Pb absorber (smaller signal).

4.4 Discussion and conclusion

X-ray bursts have been observed for positive and negative surges. We limited the field of view of a $\text{LaBr}_3(\text{Ce}^+)$ detector by a lead tube to separate ranges around the high voltage electrode, around the grounded electrode and on the space midway in between. In the case of positive surges we only detected X-rays looking in the direction of the high voltage electrode. In the case of negative surges, the EMC cabinet acted as an additional positive electrode and contributed strongly to the X-ray production if the distance was small enough, see Figure 4.6. As a result, measurements with field of view limitation were not conclusive. Still, for both surge polarities the majority of observed X-rays originated near the positive electrode.

If the X-rays are formed by collisions of high energy electrons at the anode, one would expect an increase if the aluminium surface was covered by lead (higher Z value). This has been tried, but no substantial increase was found. The amplitude or quantity of the X-rays detected remained the same, indicating that the X-ray production process is located near and not on the electrodes.

The bursts coincide in time with the large current rise on the grounded electrode, indicative for leader formation. No X-ray signals have been observed at or after the sharp rise of the current at full breakdown. The multiple bursts

indicate that the discharge develops through a stepped streamer/leader formation process. However, the signal to noise ratio, the time resolution and position of the present current probe did not allow one to distinguish corresponding steps in the currents.

We measured the current through the grounded electrode, which is the negative side of the spark gap for positive surges. It is remarkable that the X-rays then occur only when the current starts to rise to a few 100 A, whilst the primary leader forms at the (positive) high voltage electrode.

The X-ray signal is not directly related to the energy of the quanta arriving at the scintillator. It is hard to imagine quanta with energy larger than $q \cdot V_{max}$, except if a streamer ionization wave moves with the same velocity as runaway electrons in the streamer head. The observed multi-tens of megaelectronvolts signals are a pile-up of many lesser energy quanta. The few measurements with the lead absorber indicate that the bursts contain hard quanta of the order of 100 keV.

The widening of the very intense bursts has been analyzed as a train of model pulses to determine the total signal intensity. The amplitude of the first pulse was always the largest, see for instance Figure 4.5. Comparison of the signals with those from a BaF₂ detector points at saturation effects in the LaBr₃(Ce⁺) photomultiplier.

For negative surges the total energy of hard radiation strongly depended on the distance between the spark gap and the EMC cabinet, and discharge initiation was seen at the cabinet if close enough to the discharge gap. As a result, the possibility should be recognized that X-rays originate not only from the spark gap, but can also be formed elsewhere if the local electric field is large enough for discharge initiation. The experiment with repetitive streamer-corona plasma in Chapter 3 proved this. This possibility should also be considered for outdoor measurements. For positive surges, no such secondary discharges were seen which agrees with the observation that negative streamers are much harder to initiate from metal electrodes than positive ones [Bri08]. The electric field conditions are most likely met at the heads of streamers emanating from the high voltage electrode.

The average total X-ray energy from positive surges is of the order of a few hundred keV. A single quantum may be responsible for the signal or at most a few tens of quanta taking the 17 keV lower detection limit into account. Assuming isotropic emission and taking the detector solid angle $\Omega = 1.4 \times 10^{-3}$ sterad into account, one deduces that at least $4\pi/\Omega \approx 10^4$ quanta and electrons with a few hundred keV contribute to each X-ray burst, and several times this number for lesser energy quanta. This is a large number in view of current theoretical models

for the electron energy distribution [Bab03, Mos06, Li07, Tor04, Cha08] in the developing discharge, in particular if one takes into account that the electrons causing this emission are in the extreme high energy tail of the electron energy distribution.

The paper from *Rahman et al* [Rah08] also discusses X-ray production during similar discharges of a lightning surge generator, voltages of the order of 1 MV, spark gap distance of about 1 m. Their BaF₂ detector was mounted at about 1 m from the spark gap in a floating shielded cabinet. In contrast to our results only X-rays have been detected during negative surges, and also X-rays have been seen at the moment of full gap breakdown. Even with similar slightly asymmetric gaps (grounded electrode rounded disk, 8 cm diameter) we observed X-rays for both polarity. The multi-bursts shown for instance in Figure 4.3 were not reported. Both experiments show that experimental research on runaway electrons in long sparks can be performed in the laboratory. The signals are a multiple integral over the X-rays energy distribution, folded with the detector response, and their direction in space and timing folded with the detector characteristic times. To unravel the signals into an electron energy distribution function requires substantial effort.

Comments

The statement in section 4.4 ‘for both surge polarities the majority of observed X-rays originated near the positive electrode’ needs to be revised. The limitation of the field of view of the X-ray detector collimated by the lead tube was not verified. The current measurements on both electrodes presented in Chapter 5 are more conclusive. From the current measurements on both electrodes, it is evident that the X-ray burst occur at the negative electrode (the cathode) when negative streamers are formed.

The current measurements in Chapter 5 also shows that at the moment of X-ray bursts the currents on both electrodes is still small, indicating that the streamer currents have not evolved into leader currents.

CHAPTER 5

OBSERVATION OF X-RAY BURSTS IN METER-LONG DISCHARGES ASSOCIATED WITH NEGATIVE STREAMER INITIATION

Experimental results of X-ray bursts that occur during the streamer development of long spark discharges are presented in this chapter. The inter-electrode gap was 86 or 146 cm; positive and negative high voltages in the order of 1 MV were applied. A $\text{LaBr}_3(\text{Ce}^+)$ scintillation detector was used for X-ray detection during the spark formation, time synchronized with the voltage and the currents at both gap electrodes. We found that the X-ray bursts exclusively coincide with the formation of the negative streamers on the cathode, for both voltage polarities and both gap distances. The X-ray bursts detected appeared mainly on or in close approximation of the rising edge seen in the current waveform associated with negative streamers. For negative polarity with 146 cm air gap, the high voltage electrode current as function of time indicates a stepped process.

5.1 Introduction

In this chapter we focussed on the timing and localization of X-ray burst during the spark formation process. Current measurements on both electrodes allow for monitoring the different phases in the streamer channel elongation process. An optical fiber data transmission system has been designed for electrical isolation of the data acquisition of the current measured on the high voltage electrode.

5.2 Experimental set-up and procedure

The experimental condition remains approximately the same as described in Chapter 4. The measurements have been expanded with current measurement on the high voltage electrode. The electrode configuration is now vertical with the grounded electrode projecting 15 cm out from the conducting floor. Our set-up deviates from the usual high voltage point-plane (grounded) configuration in order to concentrate and measure the current at the grounded electrode. Much attention has been paid to control the electrical environment in order to avoid streamers induced near the setup, which is a possible source for X-ray emission. The EMC-cabinet has been covered by conductive plastic, flush with the security fence around the high voltage area, to avoid local streamer caused by electric field concentrations at bolts and other protruding elements. The multi-bursts of hard radiation shown in Figure 4.3(b) are not seen anymore. The 7 m distance between generator and test spark gap reduces the chance of X-ray detection from the generator switches. Both positive and negative high voltage polarities were applied.

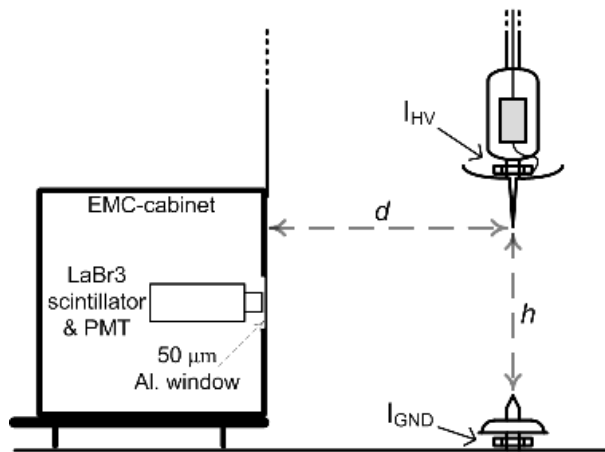


Figure 5.1: A sketch of the experimental set-up, showing the high voltage electrode at the height h above the grounded electrode, at the distance d from the $\text{LaBr}_3(\text{Ce}^+)$ scintillator detector.

Figure 5.1 shows a sketch of the electrode configuration with the position of the $\text{LaBr}_3(\text{Ce}^+)$ scintillator detector indicated. The high voltage electrode has a 21° cone angle with 0.5 mm tip radius while the grounded electrode has a 53° cone angle with 1 mm tip radius. The electrode distance h can be varied depending on the experiments; the distance d is usually 0.4 m larger than h . As in Chapter 4, the surge voltage V_{HV} at the generator is measured by a 9 m tall 1:2000

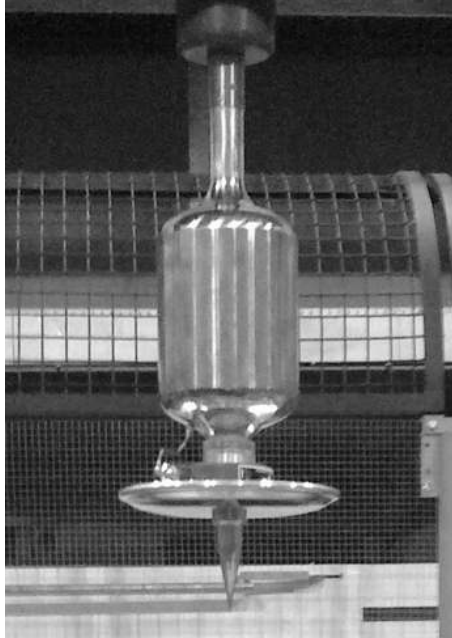


Figure 5.2: *Photograph of the high voltage electrode with current probe.*

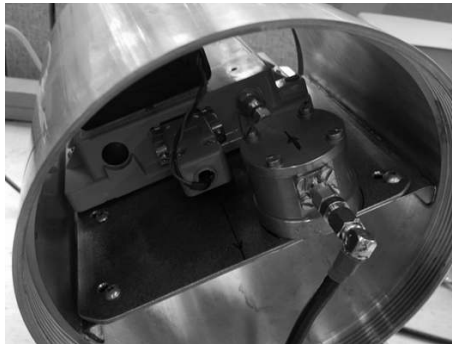


Figure 5.3: *Photograph of the optical transmitter inside the high voltage electrode.*

high voltage divider. Current probes (Pearson 7427) with 5 ns rise time and 70 MHz bandwidth incorporated on both electrodes measured the currents. The probe signal from the grounded electrode I_{GND} is fed directly to the oscilloscope (LeCroy WaveRunner 104MXi-A). The probe on the high voltage electrode I_{HV} is protected by an aluminum disk directly under the probe (Figure 5.2). The disk carries the high voltage electrode tip. The current probe signal is attenuated

and fed to an optical transmitter (Zonu Optical OZ600 with extended bandwidth from 10 kHz to 3.3 GHz) mounted inside the floating electrode casing (Figure 5.3). A 40 m single mode optical fiber then transports the signal to the receiver inside the EMC-cabinet.

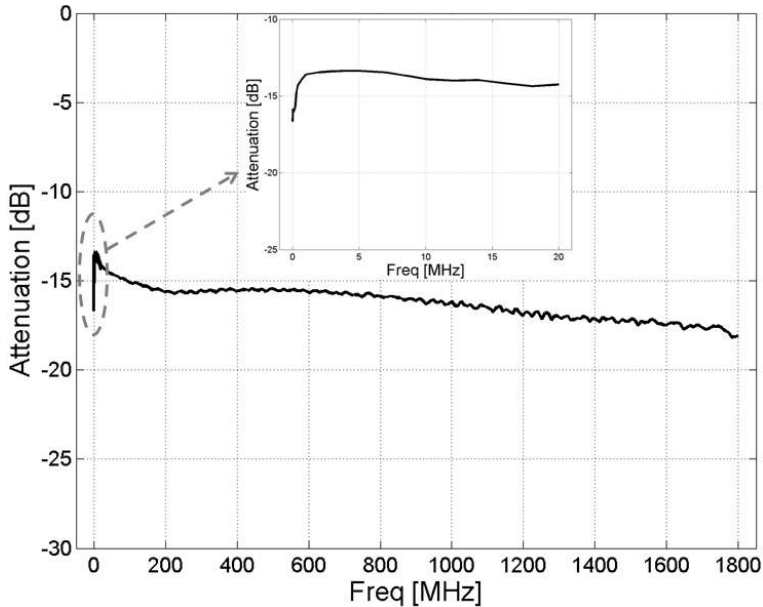


Figure 5.4: The frequency response of the optical fiber data transmission system from 10 kHz to 1.8 GHz.

Figure 5.4 shows the frequency dependence of the optical fiber data transmission system. The frequency response in the 100 kHz up to 1.8 GHz was measured with the HP 4396A network analyzer. The lower frequencies from 10 kHz up to 20 MHz were measured manually using a sine wave from the Agilent 3320A function generator and monitored on the oscilloscope (LeCroy WaveRunner 104MXi-A). These results are shown in the inset in Figure 5.4. The frequency response range measured seems to be in accordance with the specification of the manufacturer. A fast clipping diode circuit protects the optical transmitter against overvoltage from the current signal. This has been tested with the set-up shown in Figure 5.5, where two identical current probes (Pearson 7427) are stacked around the same electrode. The current signal from the upper probe is obtained directly, while the current signal from the lower probe is obtained through the optical fiber data transmission system. Figure 5.6 shows that current clipping sets in at around 380 A, but the current waveform through the optical fiber data transmission system (I_{opt}) begins to saturate at around 220 A due to saturation effects in the

diode. The overlapping of the current waveforms before 220 A confirms that the calibration factor for I_{opt} is correct. I_{opt} is attenuated twice as much as I_{GND} .



Figure 5.5: Photograph of set-up for testing the current waveform measured directly (upper probe) and the current waveform obtained through the optical fiber data transmission system (lower probe).

When the high voltage surge increases, a small capacitive current runs between the disk carrying the high voltage electrode and the environment beneath. This capacitive current can be estimated by treating the disk as part of a sphere with radius $r = 12.5$ cm. The capacitance of this sphere is:

$$C = 4\pi\epsilon_0 r \approx 14pF$$

The disk surface is $\frac{\pi r^2}{4\pi r^2} = 0.25$ of the sphere surface, thus only 25% of this capacitive current will go through the current probe. The part of the capacitive current in the I_{HV} probe signal can now be calculated by:

$$\frac{C}{4} \frac{dV}{dt} \approx 7A,$$

with $\frac{dV}{dt} = \frac{1 \cdot 10^6}{0.5 \cdot 10^{-6}} = 2 \cdot 10^{-12} \text{ V} \cdot \text{s}^{-1}$ obtained from the slope of the voltage waveform V_{HV+} in Figure 5.7. Since the capacitance of the disk and tip with respect to the environment is small, the probe senses the current in the initial streamer phase correctly.

5.3 Experimental data

The data as recorded by the oscilloscope showed resonances near the current steps and at the onset of the streamer currents with frequencies well above 70 MHz.

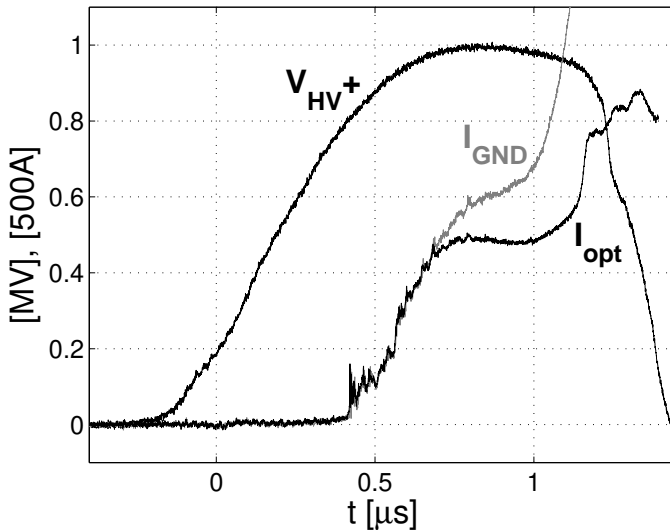


Figure 5.6: Comparison of the current waveform measured directly (I_{GND}) and the current waveform obtained through the optical fiber data transmission system (I_{opt}).

These could be actual current variations, or internal current probe resonances. Therefore, the current waveforms presented in the subsequent figures (Figures 5.7, 5.9-5.13) are shown filtered by a first order low-pass Butterworth filter with characteristic frequency of 70 MHz, the upper frequency for which the current probe is specified. Together with the 5 ns rise time of the probes, the uncertainty in the timing of the current axis is about 7 ns.

5.3.1 Results for positive high voltage surges

Figure 5.7 shows a record with positive surge over an 86 cm electrode gap distance. The voltage over the gap rises to 980 kV. The breakdown mechanism in the point-point gap starts with the formation of an impulse streamer-corona burst on the high voltage electrode at $t = 0.2 \mu\text{s}$. Streamers are formed on the anode and propagate downward to the cathode. The current leaving the grounded electrode remains zero while the anode current is developing. Approximately $0.4 \mu\text{s}$ later an upward streamer is initiated on the grounded electrode, as shown by the current waveforms. The average electric field between the electrodes is approximately $11.4 \text{ kV}\cdot\text{cm}^{-1}$ (far less than at the streamer head). Assuming the critical value for positive streamer propagation to be $5 \text{ kV}\cdot\text{cm}^{-1}$ [Baz00, Ch.2], this would mean that the cathode-directed streamer could practically bridge the

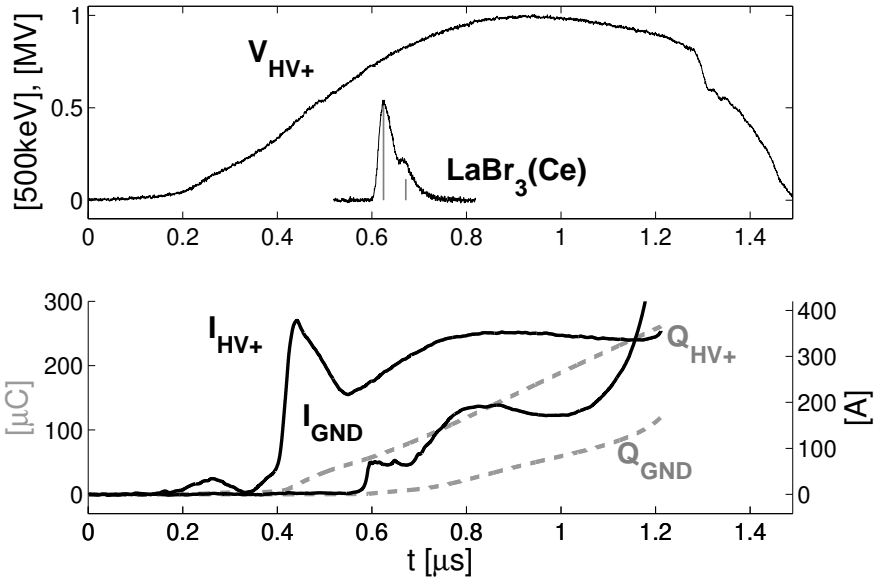


Figure 5.7: A 980 kV positive surge over 86 cm electrode distance (the X-ray signal is inverted). V_{HV+} : positive high voltage, I_{HV+} : current on positive high voltage electrode, I_{GND} : current on grounded electrode, Q_{HV+} : charge obtained from I_{HV+} and Q_{GND} : charge obtained from I_{GND} .

whole gap prior to the final jump or flashover. With this in mind, we found it more suitable to use the term streamer instead of leader here. The anode current I_{HV+} can be divided in four phases.

1. The bulge at $t = 0.25 \mu\text{s}$ is attributed to space charge build up around the anode. The current attains 33 A at the $V_{HV+} = 140 \text{ kV}$; the charge is then $1.3 \mu\text{C}$. This value agrees with the physical radius of the anode.
2. The sharp current rise near $t = 0.4 \mu\text{s}$ signals the onset of the positive streamer bursts. The current peaks at 380 A at $V_{HV+} = 440 \text{ kV}$. It apparently saturates and then rises again with constant slope up to $0.8 \mu\text{s}$.
3. The current remains nearly constant up to $1.2 \mu\text{s}$.
4. At $t = 1.2 \mu\text{s}$ the electrodes are bridged and I_{HV+} suddenly makes a jump towards the clipping level. The sudden drop in V_{HV+} at $t = 1.3 \mu\text{s}$ indicates that the conductive channel has formed between the electrodes leading to a full breakdown.

A phenomenological description of the spark discharge process based on streak photography can be found in many literatures, e.g. [Baz00, Ch.2]. Not much attention has been paid to the possibility of hard radiation emission during the spark formation. These X-ray measurements time synchronized with streamer currents are unique and have not been treated before in such detail in literature.

Of particular interest is the coincidence of the sudden onset on I_{GND} on the grounded electrode and the appearance of the X-ray signal. The coincidence occurred in 30 out of 80 measurements; in the remaining 50 no X-rays were detected. No X-ray bursts have been detected at the onset on I_{HV+} . This indicates that the energetic burst is linked with the negative upward moving streamer only. Two of the 30 records showed an additional X-ray burst within a short time after the first, as indicated by the second peak in X-ray signal shown in Figure 5.7. It can be seen that this second bursts is also accompanied by a peak in the current waveform I_{GND} . A fit to the composite X-ray signal resulted in two equivalent energies of 264 and 57 keV separated by $0.05 \mu\text{s}$. The fit procedure (described in section 4.2.1) gives the peak amplitude and the location of this peak value, but the X-ray occurs earlier at the onset of the $\text{LaBr}_3(\text{Ce}^+)$ scintillator detector pulse. This effect was shown in Figure 4.5 where the single fast response of BaF_2 on the X-ray burst coincided with the onset of the $\text{LaBr}_3(\text{Ce}^+)$ signal.



Figure 5.8: *A still photograph of a positive polarity spark discharge (please ignore the reflections on the two tubes).*

In Figure 5.7 the current I_{GND} starts about $0.2 \mu\text{s}$ after the large increase in I_{HV+} . Positive streamers form at the high voltage electrode at $t = 0.4 \mu\text{s}$. When a streamer approaches the cathode cone tip, the electric field there rises since nearly the full generator voltage (then about 700 kV) is between the streamer head and the cathode. The appearance of X-rays with hundreds of keV energy indicates that some electrons supplied by the upward negative streamer enter the run-away energy regime as considered in [Coo09]. Assuming an average positive streamer velocity of about $2 \cdot 10^6 \text{ m}\cdot\text{s}^{-1}$ [Ree95], this should happen when the positive streamer travelled 0.4 m from the high voltage electrode. The I_{HV+} peak at $0.44 \mu\text{s}$ suggests a longer path. We did not find any difference in X-ray intensity or energy when the anode was changed from aluminum into lead, suggesting that the runaway electrons collide with air molecules rather than with the anode material to generate the bremsstrahlung.

We integrated the currents to obtain the charges in the streamer, Q_{HV+} and Q_{GND} . At $t = 1.2 \mu\text{s}$, about $200 \mu\text{C}$ is stored in the positive streamer. If concentrated in a single 1 m long channel, this charge would result in electric fields of the order of $\text{MV}\cdot\text{cm}^{-1}$, which is not realistic. Therefore, the current must be shared by an appreciable number of streamer branches. A still photograph taken with a simple digital camera gives an indication of the many streamer branches (Figure 5.8). Of course many more branches exist, but here we see only the bright ones. The upward connecting negative streamers from the tip of the grounded electrode can be seen clearly. Multiple streamer channel bridging can be seen at approximately one third of the height of the gap.

One notes that the streamer current I_{HV+} is larger than I_{GND} by factor of two or more for $t < 1.1 \mu\text{s}$. The crossing of the cathode and anode currents near $t = 1.15 \mu\text{s}$ indicates that the cathode current is then mainly provided by the stored charge in the positive streamers rather than by the high voltage electrode. Only at full gap breakdown the current seen by both probes become equal, as indicated by the zero crossings of the current (not shown in the Figure). The $200 \mu\text{C}$ stored in the streamers is also equivalent to a voltage of 330 kV on the 600 pF high voltage arm of the Marx generator divider. The rest of the Marx generator (the capacitors with the 500Ω resistor in series) can only partly contribute in such a short time. The streamers are an important load on the high voltage divider. This suggests that a powerful current source as a Marx generator is needed to have sufficient number of runaways and to observe the few X-ray photons.

We increased the electrode distance to 1.46 m. The streamer phase is prolonged to over $2.5 \mu\text{s}$ (Figure 5.9). The average electric field between the electrodes is now $7.5 \text{ kV}\cdot\text{cm}^{-1}$. The current I_{HV+} is smaller than in the 0.86 m gap, most likely because of less branching. The qualitative behavior is the same. Again, the

X-ray burst coincides with the onset of the negative upward streamer. A careful look indicates that the onset of the two X-ray events coincides with the first two current peaks, the same was seen in Figure 5.7.

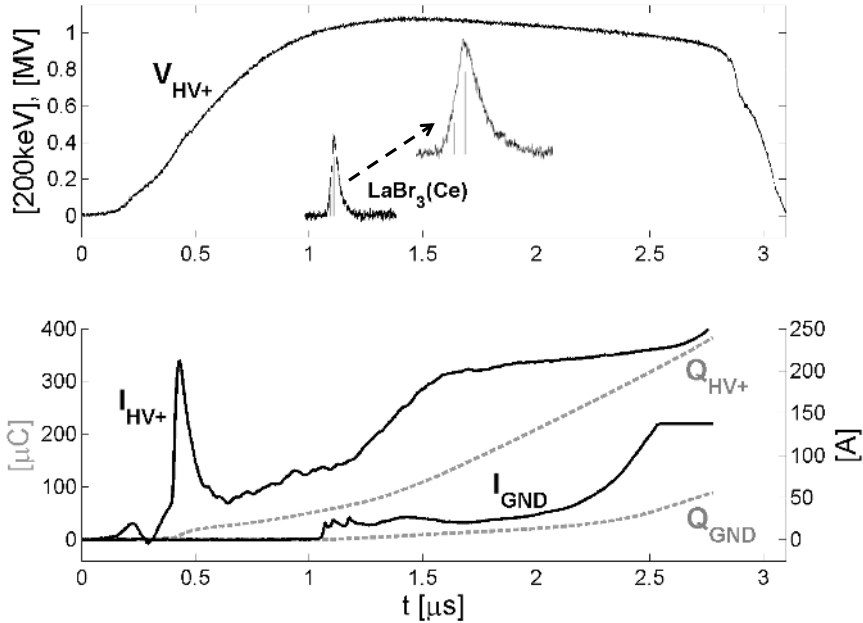


Figure 5.9: A 1.1 MV positive surge over 1.46 m electrode distance (the X-ray signal is inverted). The $\text{LaBr}_3(\text{Ce}^+)$ pulse is also shown enlarged to illustrate the double X-ray event as a result of the fit. $V_{\text{HV}+}$: positive high voltage, $I_{\text{HV}+}$: current on positive high voltage electrode, I_{GND} : current on grounded electrode, $Q_{\text{HV}+}$: charge obtained from $I_{\text{HV}+}$ and Q_{GND} : charge obtained from I_{GND} .

The currents through both electrodes differ in the begin of the discharge, this difference is larger with the increase in the electrode distance. This is caused by the Ramo-Shockley effect, the charge cloud developed around the high voltage electrode and most of the associated electric field lines are more dispersed and end in the neighborhood of the grounded electrode as sketch in Figure 5.10.

5.3.2 Results for negative high voltage surges

A record of a negative high voltage surge with -1.07 MV amplitude over an 86 cm gap is shown in Figure 5.11. The average electric field in the gap is $12.4 \text{ kV}\cdot\text{cm}^{-1}$. The discharge starts with the forming of a space charge region around

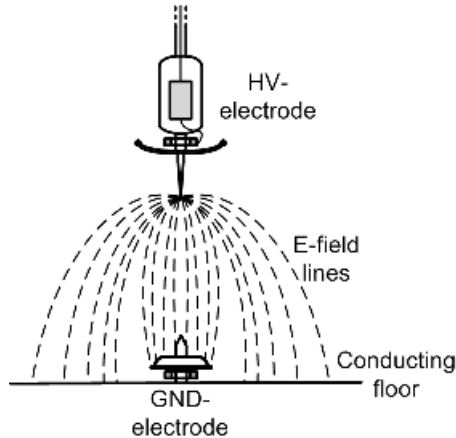


Figure 5.10: *The Ramo-Shockley effect, showing the influence of the environment on the current waveform*

the high voltage electrode. The double bulge is seen in all negative surges. This could be the result of more than one streamer corona bursts during the voltage rise (at the sharp electrode tip as intended and on the edge of the protecting disk carrying the sharp tip, see e.g. Figure 5.10). At $t = 0.5 \mu\text{s}$ streamers filaments expand from this corona area. The sharp rising edge at $t = 0.8 \mu\text{s}$ in Figure 5.11 points to a discontinuous behavior in I_{HV-} ; at least one anode directed streamer develops. Total gap breakdown occurs at $t = 1.3 \mu\text{s}$. For negative surges, the timing of X-ray bursts is less consistently linked to current steps on either electrode compared with positive surges. In 33 of a series of 50 negative surges X-ray event were registered. The current at the grounded anode is still zero when the first X-ray pulse in Figure 5.11 is recorded. It is therefore plausible to ascribe this burst of X-ray to processes related to the negative streamers from the cathode. The second X-ray pulse is remarkably synchronous with the current step from both electrodes, but this occurs rarely (only two out of 33 X-ray detection events).

Occasionally we find an intense and saturated X-ray burst (Figure 5.12), synchronized with a step in the high voltage cathode current I_{HV-} rather than anode I_{GND} . The large intensity is attributed to multiple X-ray photon detection within the response time of the scintillation detector. A fit of a standard detector response to the non-clipped data points resulted in a total energy $> 1.4 \text{ MeV}$, substantially more than attainable at 0.94 MV for a single electron. The X-ray bursts are measured real-time and each X-ray pulse is from one burst (if detected by the detector considering the small scintillation crystal surface). Saturation

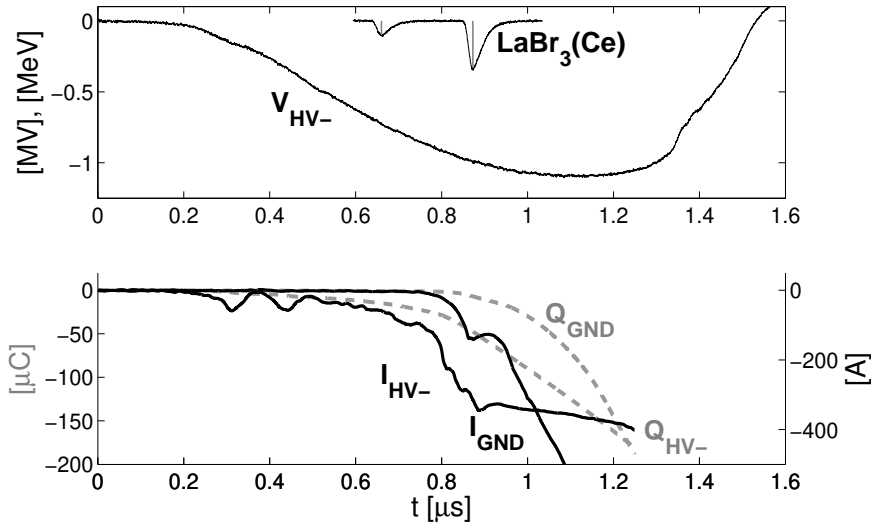


Figure 5.11: Negative surge with -1.07 MV over 86 cm electrode distance. Two X-ray bursts with 100 and 331 keV. V_{HV-} : negative high voltage, I_{HV-} : current on negative high voltage electrode, I_{GND} : current on grounded electrode, Q_{HV-} : charge obtained from I_{HV-} and Q_{GND} : charge obtained from I_{GND} .

in the $\text{LaBr}_3(\text{Ce}^+)$ scintillation crystal can be ruled out (this was confirmed by P. Dorenbos, one of developer of the material) and absorption measurement have shown a reduction in pulse amplitude. The possibility of pile-up due to the short time distribution of X-rays and photomultiplier saturation remains. The 86 cm distance negative high voltage data remained rather difficult to interpret unequivocally. The steps in the current waveforms from both electrodes are located to close in time in the measurements. This makes it difficult to draw any conclusions regarding X-ray bursts occurrences relative to these current waveforms.

At 146 cm electrode distance the average electrical field in the gap ($7.9 \text{ kV}\cdot\text{cm}^{-1}$) is lower than the critical value needed for negative streamer propagation ($10 \text{ kV}\cdot\text{cm}^{-1}$ [Baz00, Ch.2]). This means that in this case the streamer must develop into a leader in order to propagate to the anode. A typical feature of the negative spark formation is its pronounced discontinuous elongation mechanism as opposed to the positive polarity spark discharge. There are two kinds of leader channels involved: (1) the negative leader developing from the cathode itself, and (2) ahead of its tip, the ‘space leader’ propagating towards both electrodes from a point, called ‘space stem’. How a space stem is formed ahead of the main leader

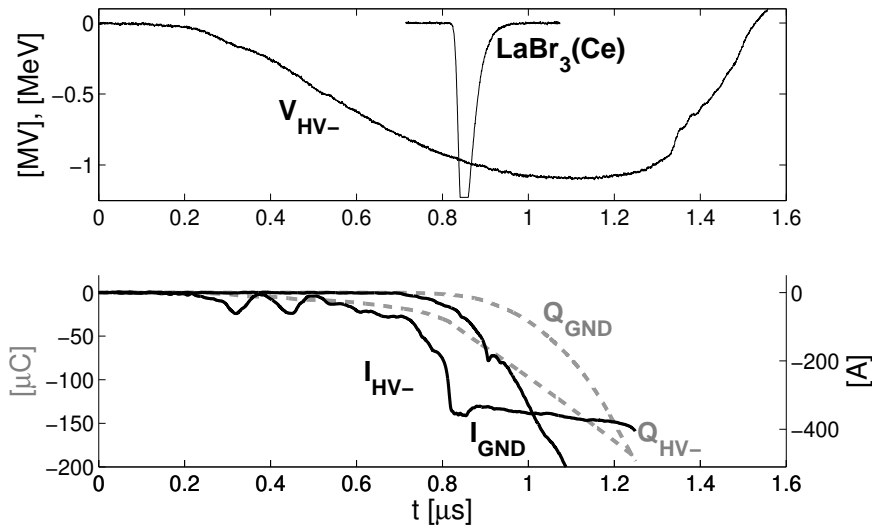


Figure 5.12: Example of multiple photon pile-up due to PMT effect. V_{HV-} : negative high voltage, I_{HV-} : current on negative high voltage electrode, I_{GND} : current on grounded electrode, Q_{HV-} : charge obtained from I_{HV-} and Q_{GND} : charge obtained from I_{GND} .

tip is still not clear. The ‘dark period’ is seen in the current waveform I_{HV-} in Figure 5.13, where at $t = 1.5 \mu\text{s}$ the current reduces back to zero. The charge buildup in the channel Q_{HV-} does not increase between $t = 1.5$ and $t = 2.85 \mu\text{s}$. At $t = 2.85 \mu\text{s}$ a pulse in I_{HV-} up to 50 A is seen, which indicate a second streamer-corona burst that could grow into a leader elongating the channel to the anode. Two X-ray signals of 0.31 and 0.50 MeV are detected during the first corona bursts, well synchronized with the step in I_{HV-} at $t = 0.8 \mu\text{s}$. No X-ray has ever been observed after the first corona burst that ends at $t = 1.5 \mu\text{s}$ or at the onset of the upward positive streamer from the anode (I_{GND}) at $t = 3 \mu\text{s}$. At $t = 3 \mu\text{s}$ one or more ascending positive streamers are initiated from the anode tip. The final spark channel is formed at $t = 5.2 \mu\text{s}$ when the downward and one of the upward moving leaders connects. At this point the voltage over the electrodes collaps.

5.4 Discussion and conclusion

Earlier measurements with a 1.5 mm lead absorber (section 4.3.5) has shown a strong reduction of the X-ray pulses compared with an unshielded detection

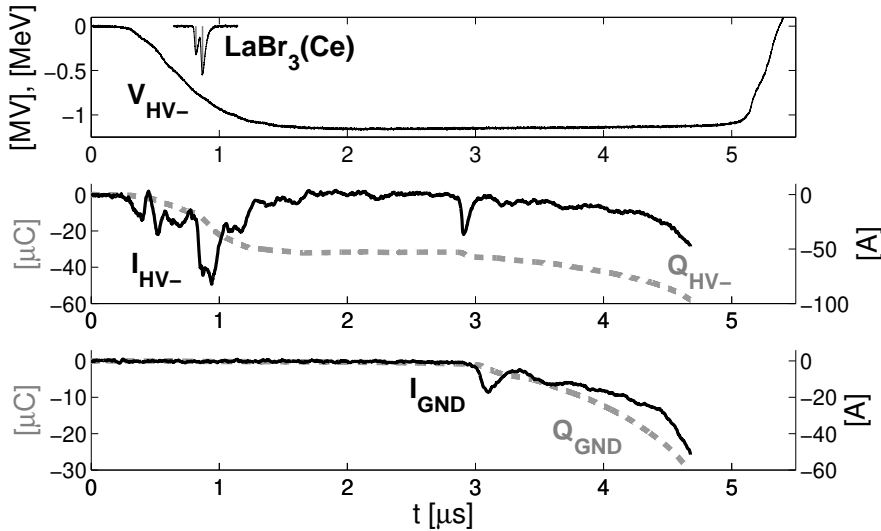


Figure 5.13: Negative surge with -1.15 MV over the 146 cm electrode distance. V_{HV-} : negative high voltage, I_{HV-} : current on negative high voltage electrode, I_{GND} : current on grounded electrode, Q_{HV-} : charge obtained from I_{HV-} and Q_{GND} : charge obtained from I_{GND} .

for negative polarity surges. This time by covering the $\text{LaBr}_3(\text{Ce}^+)$ scintillator detector with 2.5 cm lead no signal was seen during 100 surges of both polarities. This demonstrates unambiguously that the pulses measured by the $\text{LaBr}_3(\text{Ce}^+)$ scintillator detector are effectively hard radiation emanating from the surge.

When comparing the timing of X-ray detection for positive and negative polarity surges two observations can be made:

1. For positive surges X-ray bursts detection occurs when the downward positive streamer has crossed the gap substantially and induces upward negative streamers from the cathode.
2. In the case of negative polarity surges X-ray bursts were only recorded during the first streamer-corona formation, before the onset of the upward positive streamer from the anode. It can be concluded that either the local electric field in the negative streamer head or mechanism in the streamer/leader elongation is responsible for the electric field enhancement necessary for X-ray production through bremsstrahlung.

The recent observation by *Lu et al* [Lu10], suggested that the upward negative leader development of an intracloud lightning flash may be involved in the TGF

production supports our observation. *Dwyer et al* [Dwy05a] have shown explicitly that X-ray bursts are produced during the formation of the leader steps in natural negative cloud-to-ground lightning. This indicates that besides the original theory of background radiation from cosmic rays [Gur92] and the extended theory incorporating ‘relativistic feedback’ [Dwy08], the streamer/leader mechanism itself is a source for seed electrons contributing to the runaway process that produces the TGFs detected.

In this chapter we have combined the available information from streak photographs with our experimental results to gain a better insight into the processes involved during a spark formation. Without additional nanosecond-fast photography it remains difficult to interpret the measurement data. The negative streamer/leader elongation mechanism is a complex phenomenon that still needs further investigation. A solid hypothesis concerning the stepwise streamer/leader mechanism is still lacking and the continuous streak photographs used in experiments are not so straightforward for interpretation. Currently additional measurements with nanosecond-fast photography, coupled with similarly fast current sensors on both electrodes are being prepared.

CHAPTER 6

GENERAL CONCLUSIONS AND RECOMMENDATIONS

In this thesis experimental data have been gathered about conditions during metre long spark formation in air that could lead to the production of bursts of X-rays. Till now the emission of bursts of hard radiation during electrical discharges are poorly investigated. The X-ray were measured with three different scintillation detectors and a Cadmium Zinc Telluride semiconductor detector. The linearity of the $\text{LaBr}_3(\text{Ce}^+)$ was tested. The applied impuls voltage and the currents on both electrodes were monitored during the surge. An optical fiber data transmission system was integrated in the high voltage electrode in order to obtain the current waveform measured on the high voltage electrode. The electrical parameters were time synchronized with the X-ray detection. Based on these results the timing of X-ray emission with respect to the streamer current have been determined. This chapter summarizes the main findings of this thesis.

6.1 X-ray detectors

From the three scintillation detectors used in the experiments, the $\text{LaBr}_3(\text{Ce}^+)$ scintillation detector suits the most due to its combination of good energy resolution ($< 3\%$) and relatively fast decay time (16 ns). The linearity of this detector for single photon energy was verified for the experimental condition, however saturation can not be excluded when pile-up occur due to inadequate detector's time resolution. In some cases by fitting the data the problem of pile-up

could be resolved. The fast BaF₂ scintillation detector with sub-nanosecond time resolution was not able to resolve this pile-up. Results obtained with the CZT detector were too preliminary and the detection statistics were too poor to draw any conclusion from it.

6.2 X-rays from streamer-corona plasma

Soft X-rays have been detected from streamer-corona plasma with a LaBr₃(Ce⁺) scintillation detector. The short duration of the driving voltage pulse quenches the streamers before breakdown can occur. In only 0.75% of the discharges X-ray was detected, but the consistency in time of X-ray pulse detection points to the streamer-corona plasma as a source for high energetic photons. On top of that all X-ray bursts detected occurred at the start of the primary streamers. We have demonstrated experimentally that the local electric field in the vicinity of the streamer head is strong enough to accelerate electrons into the runaway regime.

6.3 Metre-long spark discharges in air

We have shown experimentally that for long spark discharges the X-ray bursts require the presence of negative streamers in the early phase of their formation. When comparing the timing of X-ray detection for positive and negative polarity surges two observations can be made:

1. In the case of positive polarity surges, the earlier onset of positive streamers from the anode does not generate high enough electric fields to produce runaway electrons. It is only till the onset of the cathode streamers that X-rays have been detected.
2. In the case of negative polarity surges X-ray emission is only registered during the initial streamer-corona burst at the cathode, not during the second streamer bursts seen in the 146 cm surges and also not at the onset of the upward positive streamers from the anode.

These observations lead to the conclusion that X-ray emission is linked to the negative streamer onset at the cathode. Unlike other experiments [Dwy05b, Rah08] we have consequently only seen bursts of X-ray during the streamer phase and not during the subsequent flashover.

The total energy deposited in the LaBr₃(Ce⁺) scintillation detector is more intense for negative polarity surges than for positive polarity surges. A plausible

explanation is that in case of negative polarity surges the cathode can be considered as a strong electron emitter to the environment. It is possible that in this case next to the expected energetic photons also secondary photons, generated by the interaction of energetic electrons with the detector's casing, contribute to the total energy detected. Absorption measurements with 1.5 mm lead have shown a strong reduction in the total energy detected.

6.4 Recommendations for future work

In future experiments it would be desirable to include nanosecond-fast photography to the measurements. The lack of this tool makes it difficult to interpret the electrical parameters obtained. Considering this area is still a subject of study, any means that could clarify the plasma condition during the X-ray bursts is welcome. The negative streamer/leader elongation mechanism is a complex phenomenon that still not resolved. A solid hypothesis concerning the stepwise leader mechanism is not available and the continuous streak photographs used in experiments remains difficult to interpretation. Future experiments should include fast photography with shot-by-shot pictures of the streamer/leader phase with short exposure time. A sequence of such pictures, compared with the available continuous streak photographs with confusing overlaps, would make the discharge process more accessible for interpretation.

As mentioned in section 2.4 it is still not clear why no multi-bursts was seen with the BaF₂ scintillation detector. This experiment deserves more attention.

Several additional measurements would contribute to a better localization of the X-ray emission:

- Faster current probes are desirable to study the fast rising edges in the negative streamer development. It is very plausible that the X-ray bursts coincide with these discontinuities as is the case for atmospheric lightning [Moo01, Dwy05a]. Some current waveforms gave indication for this, although the probes currently used are not fast enough to resolve this clearly.
- The addition of a grid sensor for electric field measurements along the discharge axis would also contribute to gain more insight in the evolution of the spark channel.
- With the measurement of spatial distribution of X-rays with multiple X-ray detectors one would be able to localize the source of X-ray emission. This result is underway.

- Experiments aiming at resolving the electron and/or photon distribution for negative polarity discharges would be interesting.

BIBLIOGRAPHY

- [ASI] “[on-line] <http://www.space.dtu.dk/english/research/projects/asim.aspx>”.
- [Bab97] N. Y. Babaeva and G. V. Naidis. “Dynamics of positive and negative streamers in air in weak uniform electric fields”. *IEEE Trans. Plasma Sci.*, vol. 25, no. 2 pp. 375–379, 1997.
- [Bab03] L. P. Babich. *High-Energy Phenomena in Electric Discharges in Dense Gases: Theory, experiment and Natural Phenomena (ISTC Science and Technology Series, vol 2)*. Futurepast, Arlington, VA, 2003.
- [Bab05] L. P. Babich, E. N. Donskoy, I. M. Kutsyk and R. A. Roussel-Dupre. “The feedback mechanism of runaway air breakdown”. *Geophys. Res. Lett.*, vol. 33, no. L09809, 2005.
- [Bab09] L. P. Babich and T. V. Loïko. “Subnanosecond pulses of runaway electrons generated in atmosphere by high-voltage pulses of microsecond duration”. *Dokl. Phys.*, vol. 54, no. 11 pp. 479–482, 2009.
- [Baz98] E. M. Bazelyan and Y. P. Raizer. *Spark Discharge*. CRC Press, New York, 1998.
- [Baz00] E. M. Bazelyan and Y. P. Raizer. *Lightning Physics and Lightning Protection*. Institute of Physics Publishing, London, 2000.
- [Bec05] K. H. Becker, U. Kogelschatz, K. H. Schoenbach and R. J. Barker. *Electrical Discharges for Environmental Purposes: Fundamentals and Applications*. Institute of Physics Publishing, Bristol, 2005.

- [Bri08] T. M. P. Briels, J. Kos, G. J. J. Winands, E. M. van Veldhuizen and U. Ebert. “Positive and negative streamers in ambient air: measuring diameter, velocity and dissipated energy”. *J. Phys. D: Appl. Phys.*, vol. 41, no. 234004, 2008.
- [Bri10] M. S. Briggs et al. “First results on terrestrial gamma ray flashes from the Fermi Gamma-ray Burst Monitor”. *Geophys. Res. Lett.*, vol. 115, no. A07323, 2010.
- [Bri11] M. S. Briggs et al. “Electron-positron beams from terrestrial lightning observed with Fermi GBM”. *Geophys. Res. Lett.*, vol. 38, no. L02808, 2011.
- [Bud09] C. Budtz-Jørgensen, I. Kuvvetli, Y. Skogseide, K. Ullaland and N. Østgard. “Characterization of CZT detectors for the ASIM mission”. *IEEE Trans. Nucl. Sci.*, vol. 56, no. 4 pp. 1842--1847, 2009.
- [Car07] B. E. Carlson, N. G. Lehtinen and U. S. Inan. “Constraints on terrestrial gamma ray flash production from satellite observation”. *Geophys. Res. Lett.*, vol. 34, no. L08809, 2007.
- [Car08] B. E. Carlson, N. G. Lehtinen and U. S. Inan. “Runaway relativistic electron avalanche seeding in the Earths atmosphere”. *J. Geophys. Res.*, vol. 113, no. A10307, 2008.
- [Cel11] S. Celestin and V. P. Pasko. “Energy and fluxes of thermal runaway electrons produced by exponential growth of streamers during the stepping of lightning leaders and in transient luminous events”. *J. Geophys. Res.*, vol. 116, no. A03315, 2011.
- [Cha08] O. Chanrion and T. Neubert. “A PIC-MCC code for the simulation of long streamer propagation at sprite altitude”. *J. Comput. Phys.*, vol. 227, no. 15 pp. 7222--7245, 2008.
- [Cha10] O. Chanrion and T. Neubert. “Production of runaway electrons by negative streamer discharges”. *J. Geophys. Res.*, vol. 115, no. A00E32, 2010.
- [Cie09] M. Ciema, D. Balabanski, M. Csatlós, J. Daugas, G. Georgiev, J. Gulyás, M. Kmiecik, A. Krasznahorkay, S. Lalkovski, A. Lefebvre-Schuhl, R. Lozeva, A. Maj and A. Vitez. “Measurements of high-energy γ -rays with LaBr₃:Ce detectors”. *Nucl. Instrum. and Meth. Phys. Res. A*, vol. 608, no. 1 pp. 76--79, 2009.

- [Coo09] V. Cooray, L. Arevalo, M. Rahman, J. Dwyer and H. Rassoul. "On the possible origin of X-rays in long laboratory sparks". *Atm. Solar-Terrestrial Phys.*, vol. 71 pp. 1890--1898, 2009.
- [Deu06] A. P. J. van Deursen, H. W. M. Smulders and R. A. A. de Graaff. "Differentiating/integrating Measurement Setup Applied to Railway Environment". *IEEE Trans. Instrum. Meas.*, vol. 55, no. 1 pp. 316--326, 2006.
- [Dor93] P. Dorenbos, J. T. M. de Haas, R. Visser, C. W. E. van Eijk and R. W. Hollander. "Absolute light yield measurements on BaF₂ crystals and the quantum efficiency of several photomultiplier tubes". *IEEE Trans. Nucl. Sci.*, vol. 40, no. 4 pp. 424--430, 1993.
- [Dor95] P. Dorenbos, J. T. M. de Haas and C. W. E. van Eijk. "Non-Proportionality in the scintillation response and the energy resolution obtainable with scintillation crystals". *IEEE Trans. Nucl. Sci.*, vol. 42, no. 6 pp. 2190--2202, 1995.
- [Dor04] P. Dorenbos, J. T. M. de Haas and C. W. E. van Eijk. "Gamma Ray Spectroscopy With a $\varnothing 19 \times \varnothing 19 \text{ mm}^3$ LaBr₃:0.5Ce³⁺ Scintillator". *IEEE Trans. Nucl. Sci.*, vol. 51, no. 3 pp. 1289--1296, 2004.
- [Dor05] P. Dorenbos. "Scintillation mechanisms in Ce⁺ doped halide scintillators". *Phys. Stat. Sol. (a)*, vol. 202, no. 2 pp. 195--200, 2005.
- [Dwy03] J. R. Dwyer. "A fundamental limit on electric fields in air". *Geophys. Res. Lett.*, vol. 30, no. 20, 2003.
- [Dwy04] J. R. Dwyer, H. K. Rassoul, M. Al-Dayeh, L. Caraway, B. Wright, A. Chrest, M. A. Uman, V. A. Rakov, K. J. Rambo, D. M. Jordan, J. Jerauld and C. Smyth. "Measurements of x-ray emission from rocket-triggered lightning". *Geophys. Res. Lett.*, vol. 31, no. L05118, 2004.
- [Dwy05a] J. R. Dwyer, H. K. Rassoul, M. Al-Dayeh, L. Caraway, A. Chrest, B. Wright, E. Kozak, J. Jerauld, M. A. Uman, V. A. Rakov, D. M. Jordan and K. J. Rambo. "X-ray bursts associated with leader steps in cloud-to-ground lightning". *Geophys. Res. Lett.*, vol. 32, no. L01803, 2005.
- [Dwy05b] J. R. Dwyer, H. K. Rassoul, Z. Saleh, M. A. Uman, J. Jerauld and J. A. Plumer. "X-ray bursts produced by laboratory sparks in air". *Geophys. Res. Lett.*, vol. 32, no. L20809, 2005.

- [Dwy05c] J. R. Dwyer and D. M. Smith. “A comparison between Monte Carlo simulations of runaway breakdown and terrestrial gamma-ray flash observations”. *Geophys. Res. Lett.*, vol. 32, no. L22804, 2005.
- [Dwy08] J. R. Dwyer. “Source mechanisms of terrestrial gamma-ray flashes”. *J. Geophys. Res.*, vol. 113, no. D10103, 2008.
- [Eac96] K. B. Eack, W. H. Beasley, W. D. Rust, T. C. Marschall and M. Stolzenburg. “Initial results from simultaneous observations of X rays and electric fields in a thunderstorm”. *J. Geophys. Res.*, vol. 101, no. D23 pp. 29673--29640, 1996.
- [Ebe06] U. Ebert, C. Montijn, T. M. P. Briels, W. Hundsdorfer, B. Meulenbroek, A. Rocco and E. M. van Veldhuizen. “The multiscale nature of streamers”. *Plasma Sources Sci. Techn.*, vol. 15 pp. S118--S129, 2006.
- [Ebe10] U. Ebert, S. Nijdam, C. Li, A. Luque, T. Briels and E. van Veldhuizen. “Review of recent results on streamer discharges and discussion on their relevance for sprites and lightning”. *J. Geophys. Res.*, vol. 115, no. A00E43, 2010.
- [Fis94] G. J. Fishman, P. N. Bhat, R. Mallozzi, J. M. Horack, T. Koshut, C. Kouveliotou, G. N. Pendleton, C. A. Meegan, R. B. Wilson, W. S. Paciesas, S. J. Goodman and H. J. Christian. “Discovery of Intense Gamma-Ray Flashes of Atmospheric Origin”. *Science*, vol. 264, no. 5163 pp. 1313--1316, 1994.
- [Gal02] I. Gallimberti. “Fundamental processes in long air gap discharges”. *C. R. Phys.*, vol. 3 pp. 1335--1359, 2002.
- [Gje10] T. Gjesteland, N. Østgaard, P. H. Connell, J. Stadsnes and G. J. Fishman. “Effects of dead time losses on terrestrial gamma ray flash measurements with the Burst and Transient Source Experiment”. *Geophys. Res. Lett.*, vol. 115, no. A00E21, 2010.
- [Gre08] B. W. Grefenstette, D. M. Smith, J. R. Dwyer and G. J. Fishman. “Time evolution of terrestrial gamma ray flashes”. *Geophys. Res. Lett.*, vol. 35, no. L06802, 2008.
- [Gur61] A. V. Gurevich. “On the theory of runaway electrons”. *Sov. Phys.*, vol. 12 pp. 904--912, 1961.
- [Gur92] A. V. Gurevich, G. M. Milikh and R. Roussel-Dupre. “Runaway electron mechanism of air breakdown and preconditioning during a thunderstorm”. *Phys. Lett. A*, vol. 165, no. A02307 pp. 463--468, 1992.

- [Ham] “[on-line] http://sales.hamamatsu.com/assets/pdf/catsandguides/pmt_handbook_v3ae.pdf”.
- [Haz09] B. J. Hazelton, B. W. Grefenstette, D. M. Smith, J. R. Dwyer, X. M. Shao, S. A. Cummer, T. Chronis, E. H. Lay and R. H. Holzworth. “Spectral dependence of terrestrial gamma-ray flashes on source distance”. *Geophys. Res. Lett.*, vol. 36, no. L01108, 2009.
- [Hou97] M. A. van Houten, E. J. M. van Heesch, A. P. J. van Deursen, R. G. Noij, J. N. A. M. van Rooy and P. C. T. van der Laan. “General methods for the protection of electronics against interferences, tested in high-voltage substations”. *Proc. 8th Int. Symp. EMC (Zürich, Switzerland)*, 1997.
- [Ilt06] A. Iltis, M. R. Mayhugh, P. Menge, C. M. Rozsa, O. Selles and V. Solovyev. “Lanthanum halide scintillators: Properties and applications”. *Nucl. Instrum. and Meth. Phys. Res. A*, vol. 563, no. 2 pp. 359–363, 2006.
- [Ina02] U. S. Inan. “Lightning effects at high altitudes: sprites, elves, and terrestrial gamma ray flashes”. *C. R. Phys.*, vol. 3 pp. 1411–1421, 2002.
- [Kai62] W. C. Kaiser, S. I. Baker, A. J. MacKay and I. S. Sherman. “Response of nai(tl) to X-rays and low energy gamma rays”. *IRE Trans. Nucl. Sci.*, vol. 9, no. 3 pp. 22–27, 1962.
- [Kho11] I. V. Khodyuk, M. S. Mikhail, J. T. M. de Haas and P. Dorenbos. “Improved scintillation proportionality and energy resolution of LaBr₃:Ce at 80 K”. *Nucl. Instrum. and Meth. Phys. Res. A*, vol. 642, no. 1 pp. 75–77, 2011.
- [Kno10] G. F. Knoll. *Radiation Detection and Measurement*. John Wiley & Sons Ltd, Chichester, 2010.
- [Kos06] I. D. Kostyrya, V. F. Tarasenko, A. N. Tkachev and S. I. Yakovlenko. “X-ray radiation due to nanosecond volume discharges in air under atmospheric pressure”. *Techn. Phys.*, vol. 51, no. 3 pp. 356–361, 2006.
- [Kuf00] E. Kuffel, J. Kuffel and W. S. Zaengl. *High Voltage Engineering: Fundamentals*. Butterworth-Heinemann, Oxford, 2000.
- [Kul98] A. A. Kulikovsky. “Positive streamer in a weak field in air: A moving avalanche-to-streamer transition”. *Phys. Rev. E*, vol. 57, no. 6 pp. 7066–7074, 1998.

- [Kum09] G. A. Kumar, I. Mazumdar and D. A. Gothe. “Experimental measurements and GEANT4 simulations for a comparative study of efficiencies of $\text{LaBr}_3:\text{Ce}$, $\text{NaI}(\text{Tl})$ and BaF_2 ”. *Nucl. Instrum. and Meth. Phys. Res. A*, vol. 610, no. 2 pp. 522--529, 2009.
- [Kuv05] I. Kuvvetli and C. Budtz-Jørgensen. “Pixelated CdZnTe Drift Detectors”. *IEEE Trans. Nucl. Sci.*, vol. 52, no. 5 pp. 1975--1981, 2005.
- [Kuv10] I. Kuvvetli, C. Budtz-Jørgensen, E. Caroli and N. Auricchio. “CZT drift strip detectors for high energy astrophysics”. *Nucl. Instrum. and Meth. Phys. Res. A*, vol. 624, no. 2 pp. 486--491, 2010.
- [Les81] Les Renardieres Group. “Negative discharges in long air gaps at les renardieres 1978 results”. *Electra*, vol. 74 pp. 67--216, 1981.
- [Li07] C. Li, W. J. M. Brok, U. Ebert and J. J. A. M. van der Mullen. “Deviations from the local field approximation in negative streamer heads”. *J. Appl. Phys.*, vol. 101, no. 123305, 2007.
- [Li09a] C. Li. *Joining particle and fluid aspects in streamer simulations*. Ph.D. thesis, Eindhoven University of Technology, 2009.
- [Li09b] C. Li, U. Ebert and W. Hundsdorfer. “3d hybrid computations for streamer discharges and production of runaway electrons”. *J. Phys. D: Appl. Phys.*, vol. 42, no. 202003, 2009.
- [Loe39] L. B. Loeb. *Fundamental Processes of Electrical Discharge in Gases*. Wiley, New York, 1939.
- [Loe41] L. B. Loeb and J. M. Meek. *The mechanism of the electric spark*. Clarendon press, Oxford, 1941.
- [Loe01] E. V. D. van Loef, P. Dorenbos, C. W. E. van Eijk, K. W. Krämer and H. U. Güdel. “High-energy-resolution scintillator: Ce^+ activated LaBr_3 ”. *Appl. Phys. Lett.*, vol. 79, no. 10 pp. 1573--1575, 2001.
- [Loe02] E. V. D. van Loef, P. Dorenbos, C. W. E. van Eijk, K. W. Krämer and H. U. Güdel. “Scintillation properties of $\text{LaBr}_3:\text{Ce}^{3+}$ crystals: fast, efficient and high-energy-resolution scintillators”. *Nucl. Instrum. and Meth. Phys. Res. A*, vol. 486, no. 1-2 pp. 254--258, 2002.
- [Lu10] G. Lu, R. J. Blakeslee, J. Li, D. M. Smith, X. M. Shao, E. W. McCaul, D. E. Buechler, H. J. Christian, J. M. Hall and S. A. Cummer. “Lightning mapping observation of a terrestrial gamma-ray flash”. *Geophys. Res. Lett.*, vol. 37, no. L11806, 2010.

- [Mar81] E. Marode. *The glow-to-arc transition in electrical breakdown and discharges in gases*, vol. 89b. Nato ASI Series B: Phys., 1981.
- [Mar05] T. C. Marshall, M. Stolzenburg, C. R. Maggio, L. M. Coleman, P. R. Krehbiel, T. Hamlin, R. J. Thomas and W. Rison. “Observed electric fields associated with lightning initiation”. *Geophys. Res. Lett.*, vol. 32, no. L03813, 2005.
- [Mar10a] V. March and J. Montanya. “Influence of the voltage-time derivative in X-ray emission from laboratory sparks”. *Geophys. Res. Lett.*, vol. 37, no. L19801, 2010.
- [Mar10b] M. Marisaldi et al. “Detection of terrestrial gamma ray flashes up to 40 MeV by the AGILE satellite”. *Geophys. Res. Lett.*, vol. 115, no. A00E13, 2010.
- [McC85] M. McCarthy and G. K. Parks. “Further observations of X-rays inside thunderstorms”. *Geophys. Res. Lett.*, vol. 12, no. 6 pp. 393--396, 1985.
- [Mee53] J. M. Meek and J. D. Cragg. *Electrical Breakdown in Gases*. Clarendon press, Oxford, 1953.
- [Mil07] B. D. Milbrath, B. J. Choate, J. E. Fast, W. K. Hensley, R. T. Kouzes and J. Schweppe. “Comparison of LaBr₃:Ce₃ and NaI(Tl) scintillators for radio-isotope identification devices”. *Nucl. Instrum. and Meth. Phys. Res. A*, vol. 572, no. 2 pp. 774--784, 2007.
- [Moo01] C. B. Moore, K. B. Eack, G. D. Aulich and W. Rison. “Energetic radiation associated with lightning stepped-leaders”. *Geophys. Res. Lett.*, vol. 28, no. 11 pp. 2141--2144, 2001.
- [Mor97] R. Morrow and J. J. Lowke. “Streamers propagation in air”. *J. Phys. D: Appl. Phys.*, vol. 30 pp. 614--627, 1997.
- [Mos06] G. D. Moss. “Monte carlo model for analysis of thermal runaway electrons in streamer tips in transient luminous events and streamer zones of lightning leaders”. *J. Geophys. Res.*, vol. 111, no. A02307, 2006.
- [Nai09] G. V. Naidis. “Positive and negative streamers in air: Velocity-diameter relation”. *Phys. Rev. E*, vol. 79, no. 5, 2009.
- [Neu08] T. Neubert, M. Rycroft, T. Farges, E. Blanc, O. Chanrion, E. Arnone, A. Odzimek, N. Arnold, C. F. Enell, E. Turunen, T. Bösinger, A. Mika, C. Haldoupis, R. J. Steiner, O. van der Velde, S. Soula, P. Berg,

- F. Boberg, P. Thejll, B. Christiansen, M. Ignaccolo, M. Füllekrug, P. T. Verronen, J. Montanya and N. Crosby. "Recent results from studies of electric discharges in the mesosphere". *Surv. Geophys.*, vol. 29 pp. 71--137, 2008.
- [Ngu08] C. V. Nguyen, A. P. J. van Deursen and U. Ebert. "Multiple x-ray bursts from long discharges in air". *J. Phys. D: Appl. Phys.*, vol. 41, no. 234012, 2008.
- [Ngu10] C. V. Nguyen, A. P. J. van Deursen, E. J. M. van Heesch, G. J. J. Winands and A. J. M. Pemen. "X-ray emission in streamer-corona plasma". *J. Phys. D: Appl. Phys.*, vol. 43, no. 025202, 2010.
- [Nij11] S. Nijdam. *Experimental Investigations on the Physics of Streamers*. Ph.D. thesis, Eindhoven University of Technology, 2011.
- [Nik06] M. Nikl. "Scintillation detectors for x-rays". *Meas. Sci. Technol.*, vol. 17, no. 4 pp. R37--R54, 2006.
- [NIS] "[on-line] <http://www.nist.gov/pml/data/xcom/index.cfm>".
- [Owe06] A. Owens, T. Buslaps, V. Gostilo, H. Graafsma, R. Hijmering, A. Kozorezov, A. Loupilov, D. Lumb and E. Welter. "Hard X- and γ -ray measurements with a large volume coplanar grid CdZnTe detector". *Nucl. Instrum. and Meth. Phys. Res. A*, vol. 563, no. 1 pp. 242--248, 2006.
- [Pam00] M. A. J. van Pamelan, C. Budtz-Jørgensen and I. Kuvvetli. "Development of CdZnTe X-ray detectors at DSRI". *Nucl. Instrum. and Meth. Phys. Res. A*, vol. 439, no. 2-3 pp. 625--633, 2000.
- [Par81] G. K. Parks, B. H. Mauk, R. Spiger and J. Chin. "X-ray enhancements detected during thunderstorm and lightning activities". *Geophys. Res. Lett.*, vol. 8, no. 11 pp. 1176--1179, 1981.
- [Pas03] V. P. Pasko. "Electric jets". *Nature*, vol. 423 pp. 927--929, 2003.
- [Qua11] F. Quarati, A. Owens, P. Dorenbos, J. de Haas, G. Benzoni, N. Blasi, C. Boiano, S. Brambilla, F. Camera, R. Alba, G. Bellia, C. Maiolino, D. Santonocito, M. Ahmed, N. Brown, S. Stave, H. Weller and Y. Wu. "High energy gamma-ray spectroscopy with LaBr₃ scintillation detectors". *Nucl. Instrum. and Meth. Phys. Res. A*, vol. 629, no. 1 pp. 157--169, 2011.

- [Rae39] H. Raether. "Die Entwicklung der Elektronenlawine in den Funkenkanal". *Z. Phys.*, vol. 112, no. 7-8 pp. 464--489, 1939.
- [Rae64] H. Raether. *Electron Avalanches and Breakdown in Gases*. Butterworths, London, 1964.
- [Rah08] M. Rahman, V. Cooray, N. A. Ahmad, J. Nyberg, V. A. Rakov and S. Sharma. "X rays from 80-cm long sparks in air". *Geophys. Res. Lett.*, vol. 35, no. L06805, 2008.
- [Rai91] Y. P. Raizer. *Gas Discharge Physics*. Springer, New York, 1991.
- [Rak03] V. A. Rakov and M. A. Uman. *Lightning: Physics and Effects*. Cambridge University Press, New York, 2003.
- [Ree95] T. Reess, P. Ortega, A. Gibert, P. Domens and P. Pignolet. "An experimental study of negative discharge in a 1.3 m point-plane air gap: the function of the space stem in the propagation mechanism". *J. Phys. D: Appl. Phys.*, vol. 28 pp. 2306--2313, 1995.
- [Rep08] A. G. Rep'ev and P. B. Repin. "Spatiotemporal Parameters of the X-ray Radiation from a Diffuse Atmospheric-Pressure Discharge". *Techn. Phys.*, vol. 53, no. 1 pp. 73--80, 2008.
- [Scia] "[datasheet] BaF₂ scintillation detectors specifications for positron life time studies".
- [Scib] "[on-line] <http://www.scionix.nl/>".
- [Sen95] D. D. Sentman, E. M. Wescott, D. L. Osborne, D. L. Hampton and M. J. Heavne. "Preliminary results from the Sprites94 aircraft campaign: 1. Red sprites". *Geophys. Res. Lett.*, vol. 22, no. 10 pp. 1205--1208, 1995.
- [Sha03] K. S. Shah, M. Klugerman, W. W. Moses, S. E. Derenzo and M. J. Weber. "LaBr₃:Ce3 Scintillators for Gamma-Ray Spectroscopy". *IEEE Trans. Nucl. Sci.*, vol. 50, no. 6 pp. 2410--2413, 2003.
- [Sha10] X. M. Shao, T. Hamlin and D. M. Smith. "A closer examination of terrestrial gamma-ray flash-related lightning processes". *Geophys. Res. Lett.*, vol. 115, no. A00E30, 2010.
- [Sha11] T. Shao, C. Zhang, Z. Niu, P. Yan, V. F. Tarasenko, E. K. Baksht, A. G. Burachenko and Y. V. Shut'ko. "Diffuse discharge, runaway electron, and x-ray in atmospheric pressure air in a inhomogeneous electrical field in repetitive pulsed modes". *Appl. Phys. Lett.*, vol. 98, no. 021503, 2011.

- [Sig84] R. S. Sigmond. “The residual streamer channel: return strokes and secondary streamers”. *J. Appl. Phys.*, vol. 56, no. 5 pp. 1355--1370, 1984.
- [Smi05] D. M. Smith, L. I. Lopez, R. P. Lin and C. P. Barrington-Leigh. “Terrestrial gamma-ray flashes observed up to 20MeV”. *Science*, vol. 307, no. 1085 pp. 1085--1088, 2005.
- [Sta67] Y. L. Stankevich and V. G. Kalinin. “Fast electrons and X-ray radiation during the initial stage of growth of a pulsed spark discharge in air”. *Sov. Phys. Dokl.*, vol. 12, no. 11 pp. 1042--1043, 1967.
- [StG] “[on-line] <http://www.detectors.saint-gobain.com/>”.
- [Tak11] A. Takada, H. Kubo, H. Nishimura, K. Ueno, K. Hattori, S. Kabuki, S. Kurosawa, K. Miuchi, E. Mizuta, T. Nagayoshi, N. Nonaka, Y. Okada, R. Orito, H. Sekiya, A. Takeda and T. Tanimori. “Observation of diffuse cosmic and atmospheric gamma rays at balloon altitudes with an electron-tracking Compton camera”. *Astrophys. J.*, vol. 773, no. 1, 2011.
- [Tar02] P. Tardiveau, E. Marode and A. Agneray. “Tracking an individual streamer branch among others in a pulsed induced discharge”. *J. Phys. D: Appl. Phys.*, vol. 35 pp. 2823--2829, 2002.
- [Tor04] T. Torii, T. Nishijima, Z.-I. Kawasaki and T. Sugita. “Downward emission of runaway electrons and bremsstrahlung photons in thunderstorm electric fields”. *Geophys. Res. Lett.*, vol. 31, no. L05113, 2004.
- [Vel00] E. M. van Veldhuizen. *Electrical Discharges for Environmental Purposes: Fundamentals and Applications*. Nova Science, Huntington, NY, 2000.
- [Wag07] E. Wagenaars, M. D. Bowden and G. M. W. Kroesen. “Measurements of Electric-Field Strengths in Ionization Fronts during Breakdown”. *Phys. Rev. Lett.*, vol. 98, no. 075002 pp. 3010--3017, 2007.
- [Wil24] C. T. R. Wilson. “The electric field of a thundercloud and some of its effects”. *Proc. Phys. Soc. London*, vol. 37 pp. 32D--37D, 1924.
- [Win06a] G. J. J. Winands, Z. Liu, A. J. M. Pemen, E. J. M. van Heesch, K. Yan and E. M. van Veldhuizen. “Temporal development and chemical efficiency of positive streamers in a large scale wire-plate reactor as a function of voltage waveform parameters”. *J. Phys. D: Appl. Phys.*, vol. 39, no. 14 pp. 3010--3017, 2006.

- [Win06b] G. J. J. Winands, K. Yan, A. J. M. Pemen, S. A. Nair, Z. Liu and E. J. M. van Heesch. “An industrial streamer corona plasma system for gas cleaning”. *IEEE Trans. Plasma Sci.*, vol. 34, no. 5 pp. 2426–2433, 2006.
- [Win07] G. J. J. Winands. *Efficient Streamer Plasma Generation*. Ph.D. thesis, Eindhoven University of Technology, 2007.
- [Win08] G. J. J. Winands, Z. Liu, A. J. M. Pemen and K. Yan. “Analysis of streamer properties in air as function of pulse and reactor parameters by ICCD photography”. *J. Phys. D: Appl. Phys.*, vol. 41, no. 23 pp. 3010–3017, 2008.
- [Yan98] K. Yan, H. Hui, M. Cui, J. Miao, X. Wu, C. Bao and R. Li. “Corona induced non-thermal plasmas: fundamental study and industrial applications”. *J. Electrostat.*, vol. 44, no. 1-2 pp. 17–39, 1998.

LIST OF PUBLICATIONS

Journal publications

- [1] C.V. Nguyen , A.P.J. van Deursen, E.J.M. van Heesch, G.J.J. Winands, A.J.M. Pemen. “X-ray emission in pulsed streamer-corona plasma”. *J. Phys. D: App. Phys.*, vol. 43, no. 2, 25202 (5p), 2010.
- [2] C.V. Nguyen, A.P.J. van Deursen, U.M. Ebert. “Multiple x-ray bursts from long discharges in air”. *J. Phys. D: App. Phys.*, vol. 41, no. 23, 234012 (7p), 2008.

Conference publications

- [1] G. Bargboer, A.P.J. van Deursen, C.V. Nguyen, H.T. Steenstra, T. Bosveld, R. Parrado Curros, J.P.M. Broekmeulen. “Finding weak spots in lightning protection”. In *Proceedings Int. Symp. on EMC (EMC Europe '08)*, pp. 269-274. Hamburg, Germany, 2008.

Conference and workshop contributions

Talks

- Oct. 2010 “Hard radiation from long spark discharges”. *Workshop on TLE's and TGF's*, CWI, Amsterdam, The Netherlands.
- May 2009 “X-ray Burst in Long Discharges”. *AGU Chapman Conference on Effects of Thunderstorms and Lightning in the Upper Atmosphere*, The Pennsylvania State University, University Park, Pennsylvania, US.

- Jun. 2008 “X/ γ -ray Detection During Streamer Development (in Ambient Air)”. *Workshop on Coupling of Thunderstorms and Lightning Discharges to Near-Earth Space*, University of Corsica, Corte, France.
- Oct. 2007 “MeV γ 's from long leaders in STP air”. *Workshop on Streamers Sprites, Leaders, Lightning: from micro- to macroscales*, Lorentz Center, Leiden, The Netherlands.
- Mar. 2007 “MeV γ 's from long streamers in STP air”. *19th NNV/CPS Symposium on Plasma Physics and Radiation Technology*, Lunteren, The Netherlands.

Posters

- Jun. 2008 *The 35th IEEE International Conference on Plasma Science*, Karlsruhe, Germany.
- Mar. 2008 *20th NNV/CPS Symposium on Plasma Physics and Radiation Technology*, Lunteren, The Netherlands.

ACKNOWLEDGEMENTS

The work presented in this thesis would not have been possible without the support and contribution of many people from different areas.

In the first place, I would like to express my sincere gratitude to my direct supervisor Lex van Deursen. This work could not have been established without his great support and the necessary guidance throughout this project.

A very big thank to my promotoren prof.dr.ir. Jan Blom and prof.ir. Wil Kling for their support and encouragements. In addition, I would like to thank the committee members for taking the time to read and give comments on my thesis. Special thanks to prof.dr Ute Ebert for her involvement throughout this project and for the interesting discussions on this topic.

I would like to thank P. van Rijsingen of the Radboud University in Nijmegen for the loan of the NaI(Tl) scintillation detector. Many thanks to Carl Budtz-Jørgensen and Irfan Kuvvetli from the ASIM project for bringing the CZT detector along for experiments. It was an interesting experience. Furthermore, I thank Gilles Moerdijk from the Radiation Protection Department (SBD) for assisting us with the calibration of the X-ray detectors and giving us access to their equipment.

Performing high voltage experiments in a high voltage laboratory is something that one cannot do alone. I had a lot of help from Hennie van der Zanden with getting several equipment working properly, and Sjoerd van Driel for assisting in putting the experimental set-up together. I also got a lot of support from people in the Pulsed Power group with the streamer-corona plasma experiment and for the scientific and personal discussions: Guus Pemen, Bert van Heesch, Hans Winands, Liu Zhen, Wilfred Hoeben and Frank Beckers. Thank you all.

I would also like to thank all my friends (and colleagues) in the Electrical Energy Systems group for the enjoyable time and for not complaining about the loud ‘explosions’ I made in the laboratory.

Last but not least, I’m grateful to my family for their support throughout the years.

CURRICULUM VITAE

C.V. Nguyen (Vuong) was born on 25-01-1980 in Phu Khanh (Vietnam). After finishing pre-university education in 1999 at Maas Waal College in Wijchen (The Netherlands), he studied Electrical Engineering at Eindhoven University of Technology. He received his MSc. in Electrical Engineering from Eindhoven University of Technology in 2007.

From 2006 to 2008 he was an education/research assistant at the department of Electrical Engineering in the Electrical Energy Systems group. His activities comprised: participating in the ILDAS project (designing sensors for recording lightning strikes on airplanes), on-site testing of grounding system of a building, assisting in courses and investigating spark discharges in the high voltage laboratory.

In 2008 his work turned into a PhD project of which the results are presented in this dissertation.